JOURNAL OF PETROLOGY | VOLUME 53 | NUMBER 5 | PAGES 919–948 | 2012 | doi:10.1093/petrology/egs003

Two-Stage, Extreme Albitization of A-type Granites from Rajasthan, NW India

PARAMPREET KAUR[1,2]*, NAVEEN CHAUDHRI[1], ALBRECHT W. HOFMANN[2], INGRID RACZEK[2], MARTIN OKRUSCH[3], SUSANNE SKORA[4] AND LUKAS P. BAUMGARTNER[4]

[1]CENTRE OF ADVANCED STUDY IN GEOLOGY, PANJAB UNIVERSITY, CHANDIGARH-160 014, INDIA

[2]MAX-PLANCK-INSTITUT FÜR CHEMIE, POSTFACH 3060, 55020 MAINZ, GERMANY

[3]LEHRSTUHL FÜR GEODYNAMIK UND GEOMATERIALFORSCHUNG, INSTITUT FÜR GEOGRAPHIE UND GEOLOGIE, UNIVERSITÄT WÜRZBURG, AM HUBLAND, 97074 WÜRZBURG, GERMANY

[4]INSTITUTE OF MINERALOGY AND GEOCHEMISTRY, UNIVERSITY OF LAUSANNE, CH-1015 LAUSANNE, SWITZERLAND

RECEIVED JUNE 10, 2008; ACCEPTED JANUARY 05, 2012
ADVANCE ACCESS PUBLICATION FEBRUARY 10, 2012

Albitization is a common process during which hydrothermal fluids convert plagioclase and/or K-feldspar into nearly pure albite; however, its specific mechanism in granitoids is not well understood. The c. *1700 Ma A-type metaluminous ferroan granites in the Khetri complex of Rajasthan, NW India, have been albitized to a large extent by two metasomatic fronts, an initial transformation of oligoclase to nearly pure albite and a subsequent replacement of microcline by albite, with sharp contacts between the microcline-bearing and microcline-free zones. Albitization has bleached the original pinkish grey granite and turned it white. The mineralogical changes include transformation of oligoclase ($\sim An_{12}$) and microcline ($\sim Or_{95}$) to almost pure albite ($\sim An_{0\cdot5-2}$), amphibole from potassian ferropargasite (X_{Fe} 0·84–0·86) to potassic hastingsite (X_{Fe} 0·88–0·97) and actinolite (X_{Fe} 0·32–0·67), and biotite from annite (X_{Fe} 0·71–0·74) to annite (X_{Fe} 0·90–0·91). Whole-rock isocon diagrams show that, during albitization, the granites experienced major hydration, slight gain in Si and major gain in Na, whereas K, Mg, Fe and Ca were lost along with Rb, Ba, Sr, Zn, light rare earth elements and U. Whole-rock Sm–Nd isotope data plot on an apparent isochron of 1419 ± 98 Ma and reveal significant disturbance and at least partial resetting of the intrusion age. Severe scatter in the whole-rock Rb–Sr isochron plot reflects the extreme Rb loss in the completely albitized samples, effectively freezing $^{87}Sr/^{86}Sr$ ratios in the albite granites at very high values (0·725–0·735). This indicates either infiltration of highly radiogenic Sr from the country rock or, more likely, radiogenic ingrowth during a considerable time lag (estimated to be at least 300 Myr) between original intrusion and albitization. The albitization took place at ~350–400°C. It was caused by the infiltration of an ascending hydrothermal fluid that had acquired high Na/K and Na/Ca ratios during migration through metamorphic rocks at even lower temperatures in the periphery of the plutons. Oxygen isotope ratios increase from $\delta^{18}O = 7‰$ in the original granite to values of 9–10‰ in completely albitized samples, suggesting that the fluid had equilibrated with surrounding metamorphosed crust. A metasomatic model, using chromatographic theory of fluid infiltration, explains the process for generating the observed zonation in terms of a leading metasomatic front where oligoclase of the original granite is converted to albite, and a second, trailing front where microcline is also converted to albite. The temperature gradients driving the fluid infiltration may have been produced by the high heat production of the granites themselves. The confinement of the albitized granites along the NE–SW-trending Khetri lineament and the pervasive nature of the albitization suggest that the albitizing fluids possibly originated during reactivation of the lineament. More generally, steady-state temperature gradients induced by the high internal heat production of A-type granites may provide the driving force for similar metasomatic and ore-forming processes in other highly enriched granitoid bodies.*

KEY WORDS: *A-type metaluminous granites; albitization; infiltration metasomatism; Rajasthan, NW India; Sr–Nd–O isotopes*

*Corresponding author. E-mail: param.geol@gmail.com

INTRODUCTION

Albitization in granitoids causes an overall change in bulk composition dominated by the production of Na-rich minerals in the rock with a concomitant removal of K by the fluid. The Na-rich fluid can induce albitization by transforming any Ab–Or–An solid solution into nearly pure albite (Perez & Boles, 2005). Albitization was studied at least as far back as the early 20th century (e.g. Anderson, 1937), and affects enormous tracts of the Earth's crust ranging from sedimentary basins to magmatic systems (e.g. Carten, 1986; Cathelineau, 1986; Perez & Boles, 2005; Engvik *et al.*, 2008; Plümper & Putnis, 2009; Norberg *et al.*, 2011, among others). During albitization the original textures of the granitoid rocks may remain well preserved, even after complete alteration of the primary mineralogy (e.g. Nijland & Touret, 2001). The metasomatic process may also cause severe leaching of rare earth elements (REE) and other trace elements from the albitized granitoids. For example, the REE depletion may be related to the transformation of accessory phases, such as monazite to apatite and thorite in some peraluminous albitized granitoids (Boulvais *et al.*, 2007), whereas transformation of K-feldspar and calcic plagioclase to albite causes severe depletion in Rb, Ba, Pb and Sr. These various chemical changes are likely to be predominantly caused by fluid infiltration rather than diffusion processes. A formal model of infiltration metasomatism applied to alkali feldspars has been formulated by Hofmann (1972), following the general theory of metasomatism developed by Korzhinskii (e.g. Korzhinskii, 1968). Such alteration processes are also of economic significance because they are often spatially associated with U, Sn–W and Fe oxide–Cu–Au (IOCG) mineralization (e.g. Charoy & Pollard, 1989; Porto da Silveira *et al.*, 1991; Barton & Johnson, 1996; Mark, 1998; Williams *et al.*, 2005, and references therein).

Albitization is commonly accompanied by quartz dissolution (episyenitization), despite some secondary silicification (Cathelineau, 1986; Charoy & Pollard, 1989; Petersson & Eliasson, 1997; Costi *et al.*, 2002; Boulvais *et al.*, 2007). We present here an example of albitization that is accompanied by silicification rather than the commonly recognized desilicification.

If such metasomatized rocks are studied in isolation, this may lead to misinterpretation of their classification and origin (e.g. Elburg *et al.*, 2001). Thus, proper characterization of metasomatic alteration demands comparison of altered with unaltered samples to ascertain the original rock composition, texture and structure. Such an approach has proved to be useful to recognize the derivation of some of the trondhjemites of North America, South Australia and South Italy at the expense of the original granitoid protolith via pervasive Na-metasomatism (Drummond *et al.*, 1986; Elburg *et al.*, 2001; Fiannacca *et al.*, 2005). These studies suggest that, under appropriate geological conditions, metasomatism can affect large volumes of rock and produce highly distinctive rock types.

Albitized rocks crop out widely in the Khetri complex of the northern Aravalli mountain range, which constitutes an important Proterozoic IOCG metallogenic terrane (Knight *et al.*, 2002) in the NW Indian plate (Fig. 1). Das Gupta (1968) recorded albitization of some of the granitoids and associated metasediments (also see Jain *et al.*, 1999), and Basu & Narsayya (1983) reported alkali metasomatism along a NE–SW lineament along the eastern fringe of the Khetri region. Detailed geochemical and geochronological (U–Pb and Pb–Pb zircon dating) investigations on granitoids of the Khetri complex led to the recognition of ~1700 Ma A-type alkali-feldspar granites, comprising completely albitized granites and relatively less affected microcline–albite granites (Chaudhri *et al.*, 2003; Kaur *et al.*, 2006, 2007, 2011*a*). In this study, we present a comprehensive petrological and geochemical characterization of these albitized granitoids, and a specific, though simplified model for their origin, based on the concept of infiltration metasomatism. This model explains the two distinct steps of albitization in terms of two metasomatic fronts, which advance through the original granite simultaneously, but at different rates.

We use the Dosi pluton of the northern Khetri complex (Fig. 1b) as a characteristic example of the albitization process and the accompanying silicification, because here albitized granites occur in association with the original granites within the same pluton. We compare the results from the Dosi pluton with those from other albitized granitoids of the region to give a more comprehensive characterization of the metasomatic process that occurred on a regional scale.

GEOLOGICAL OUTLINE

In the Aravalli mountain range (Fig. 1a), Palaeoproterozoic (1850–1700 Ma) granitoid plutons are widespread in the northern segment of the Delhi fold belt (Mukhopadhyay *et al.*, 2000; Biju-Sekhar *et al.*, 2003; Kaur *et al.*, 2007, 2009, 2011*a*). Along with the Aravalli fold belt, they are part of a deformed and metamorphosed Proterozoic cover sequence over an Archaean basement (the Banded Gneissic Complex) formed by an association of metasedimentary schists, gneisses and amphibolites with granitoid intrusions (Fig. 1a; Gupta *et al.*, 1997; Sinha-Roy *et al.*, 1998; Roy & Jakhar, 2002). The majority of the granitoid plutons in the Khetri and Alwar regions of the northern Delhi fold belt are typically A-type in nature, spanning an age range of 1720–1700 Ma (Biju-Sekhar *et al.*, 2003; Kaur *et al.*, 2007, 2011*a*).

Our study focuses on the northeastern block of the Khetri complex that exposes several granitoid plutons (Fig. 1b). The traditional stratigraphic scheme established for the rocks in the Khetri region includes two divisions of

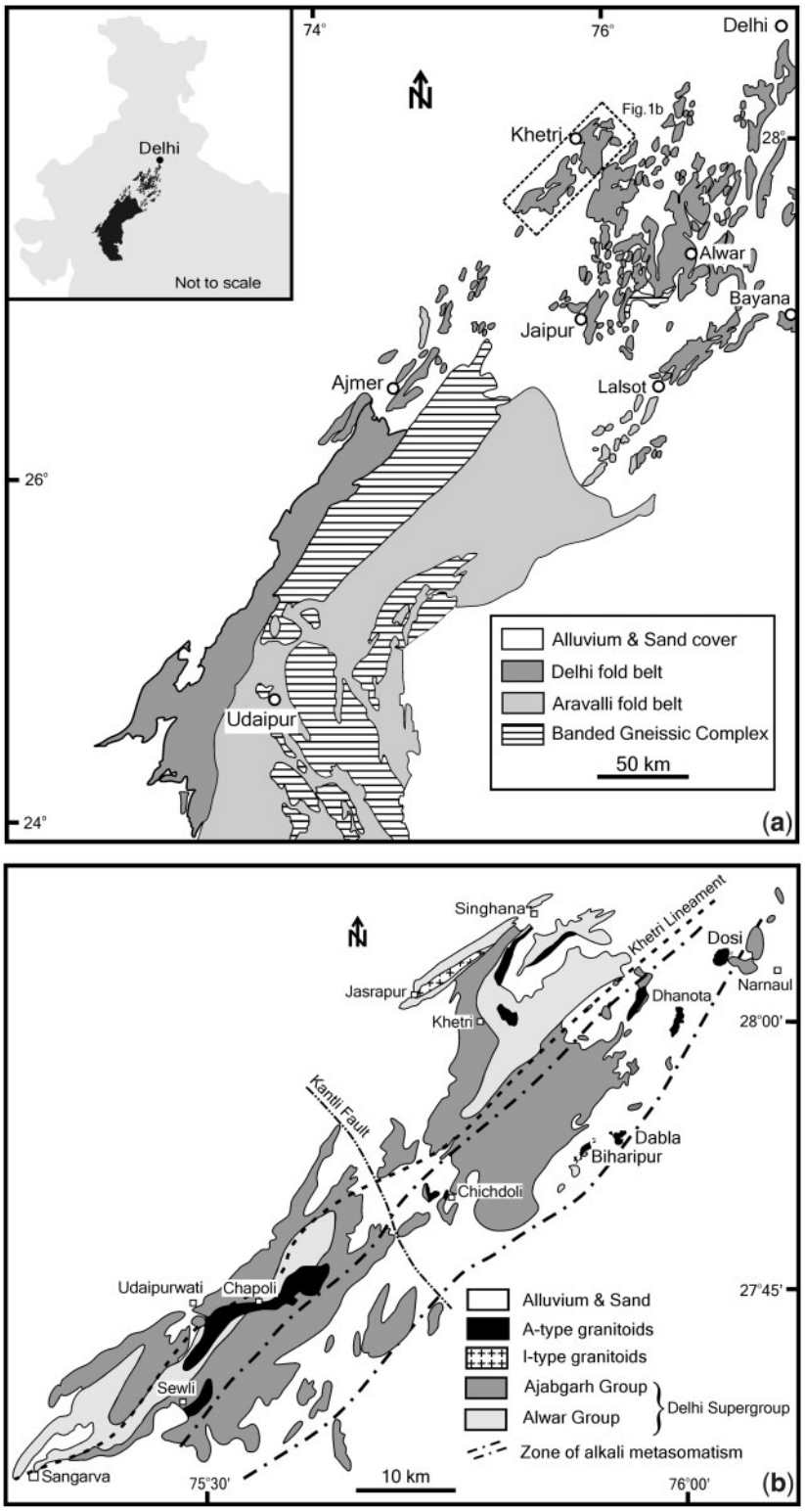

Fig. 1. (a) Simplified geological map of a part of the Aravalli mountain range showing the major Precambrian rock units (after Roy, 1988; Roy & Jakhar, 2002). Inset map shows location of the Aravalli mountain range in northwestern India, and dashed box illustrates the location of (b). (b) Generalized geological map of the Khetri complex showing locations of various granitoid plutons and lineaments (compiled from Heron, 1923; Geological Survey of India, 1997; Yadav *et al.*, 2000; and our own observations).

the Delhi Supergroup, an older unit (the Alwar Group) comprising mainly meta-arenites with metavolcanic rocks, and a younger unit (the Ajabgarh Group) consisting mainly of metapelites with metavolcanic roks (Heron, 1923; Das Gupta, 1968). These rocks form the cover sequence of a basement that mainly comprises *c.* 1700 Ma albitized A-type granites and *c.* 1850 Ma subduction-related granitoids (Kaur *et al.*, 2011*b*). The maximum age of sedimentation in the Khetri basin is ~1710 Ma (Kaur *et al.*, 2011*b*), and these sediments were regionally metamorphosed to amphibolite facies (550–600°C at 300–500 MPa; Lal & Shukla, 1975; Sarkar & Dasgupta, 1980) at around 950 Ma (Pant *et al.*, 2008). The metasomatic activity in the region is considered to post-date the regional metamorphism (Knight *et al.*, 2002). An important feature in the present context is a NE–SW lineament (the Khetri lineament), a NW–SE lineament (the Kantli lineament or fault), and an over 170 km long NNE–SSW-trending zone of albitites formed by alkali metasomatism (Fig. 1b; Ray, 1990; Yadav *et al.*, 2000).

The samples for the present study were collected from three small (2–3 km^2) granitoid intrusions located near the villages of Biharipur, Dabla and Dosi (Figs 1b and 2). The detailed field relations of the Biharipur–Dabla plutons have been presented elsewhere (Chaudhri *et al.*, 2003; Kaur *et al.*, 2006) and their field attributes relevant to the present study are viewed here mainly in comparison with those of the Dosi pluton. The latter is the northernmost granitoid body of the Aravalli mountain range, and is located about 24 km NE of Khetri town (Fig. 1b). It is an oval-shaped outcrop, *c.* 2 km × 1·4 km and, like Biharipur–Dabla, it is exposed amidst Quaternary sand and alluvium (Fig. 2). The pluton is aligned in a NNE–SSW direction in apparent northeastern continuity with the A-type Biharipur–Dabla intrusions. Dey (1985) suggested that the scattered and isolated outcrops of the Ajabgarh metasediments bear the imprints of three phases of folding, and the Dosi pluton was presumably emplaced along an anticlinal core during the late syn-kinematic phase. The petrology and geochemistry of this pluton and its relationship with regional tectonics have so far remained unexplored.

Dosi shares many similarities with the Biharipur pluton. The dominant facies, which covers ~90% of the exposed outcrop area, is represented by a pink to greyish pink microcline–albite granite (nomenclature after Streckeisen, 1976). It is a leucocratic, homogeneous and foliated rock. The trend of the foliation is NE–SW with southeasterly dips (30–65°) in conformity with those of Biharipur. In addition, a grey coloured, somewhat banded, foliated microcline–oligoclase granite (*sensu stricto*) with occasional pink phenocrysts (maximum size 1 cm) of K-feldspar (Fig. 3a) crops out locally as small patches (maximum size 100 m × 50 m) along the southwestern and northwestern margins of the pluton (Fig. 2a). Microcline-free albite granite is a subordinate facies, which is exposed along the margins of the Dosi pluton. It is white in colour, homogeneous and unfoliated. Direct contacts between microcline–albite granite and albite granite are observed particularly in Dabla. These contacts are always sharp (Fig. 3b). A subordinate transitional variety between microcline–albite granite and albite granite is also exposed. It is generally white in colour and foliated (Fig. 2a; sample DS-13); this variety is more common in the Dabla pluton where it is largely pinkish white in colour. A minor commingled zone of the albite granite and gabbroic rocks, which is best exposed in the Biharipur pluton (Fig. 2b), has also been observed along the southwestern margin of the Dosi pluton. Dykes and patches of pink-coloured microgranite occur within all the granite facies. Pods and veins or veinlets of quartz, and later pegmatite dykes are common in these plutons.

ANALYTICAL METHODS

Samples for whole-rock and isotope geochemistry were prepared following the procedure outlined by Kaur *et al.* (2006). Mineral and whole-rock analytical details for the Biharipur and Dabla plutons have been outlined by Kaur *et al.* (2006). For the Dosi pluton, mineral analyses were performed at the Mineralogisches Institut, University of Würzburg and at the Max-Planck-Institut für Chemie, Mainz, Germany. The analytical details have been given by Kaur *et al.* (2006, 2009). Back-scattered electron (BSE) images were taken at the Panjab University, Chandigarh using a JEOL JSM-6490 scanning electron microscope (SEM). Mineral abbreviations used are those by Kretz (1983). Major and trace elements were analysed at the Mineralogisches Institut, University of Würzburg, using a Philips PW 1480 X-ray fluorescence (XRF) spectrometer (for details see Kaur *et al.*, 2006). REE as well as Hf, Ta and U concentrations of the samples were obtained from Activation Laboratories Ltd., Ontario, Canada by inductively coupled plasma mass spectrometry (ICP-MS), using a Perkin Elmer SCIEX ELAN 6000 system. Duplicate measurements of sample DS15 provided a precision generally better than 2% (SD) except for Er and Lu (<4%). The accuracy of the analyses was monitored by many international reference materials (e.g. W2, WMG1, STM1, DNC1, BIR1, SY3). Based on the rock standard STM1, accuracy was usually better than 5%, except for La, Er (<10%) and Pr (<30%).

Sm–Nd and Rb–Sr isotopic analyses were carried out at the Max-Planck Institut für Chemie, Mainz. For the analysis, 100 mg of the whole-rock sample and 50 mg of the BCR2 standard were used, following the procedure outlined by Kaur *et al.* (2009). Total procedural blanks were <170 pg for Nd, <60 pg for Sm, <60 pg for Rb and

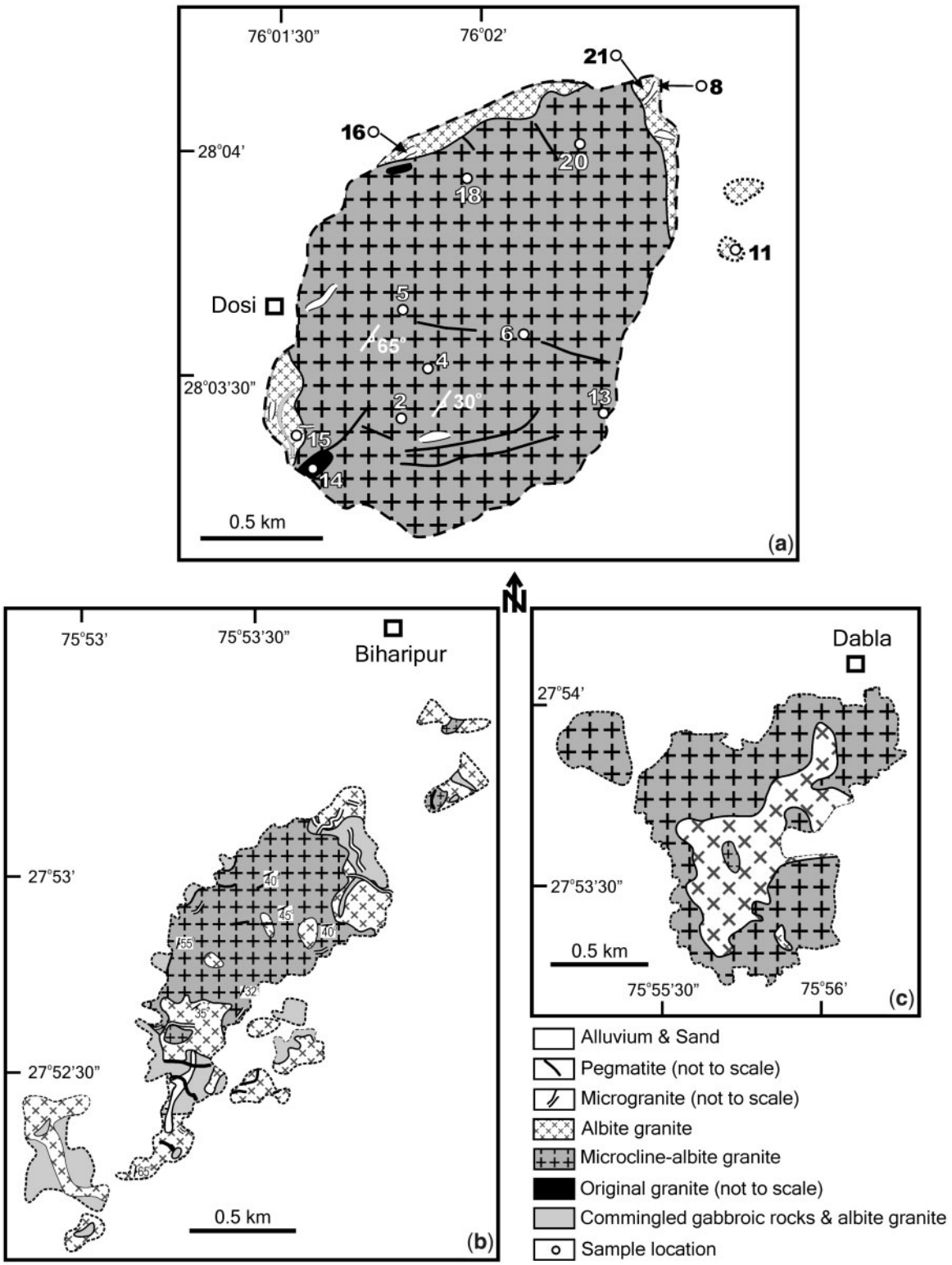

Fig. 2. Detailed geological maps of the granite bodies at (a) Dosi, (b) Biharipur (Kaur *et al.*, 2006) and (c) Dabla (Chaudhri *et al.*, 2003) showing the distribution of original and albitized granite facies and the locations of representative samples for the Dosi pluton. Sample locations for the Dabla and Biharipur plutons have been given by Chaudhri *et al.* (2003) and Kaur *et al.* (2006), respectively.

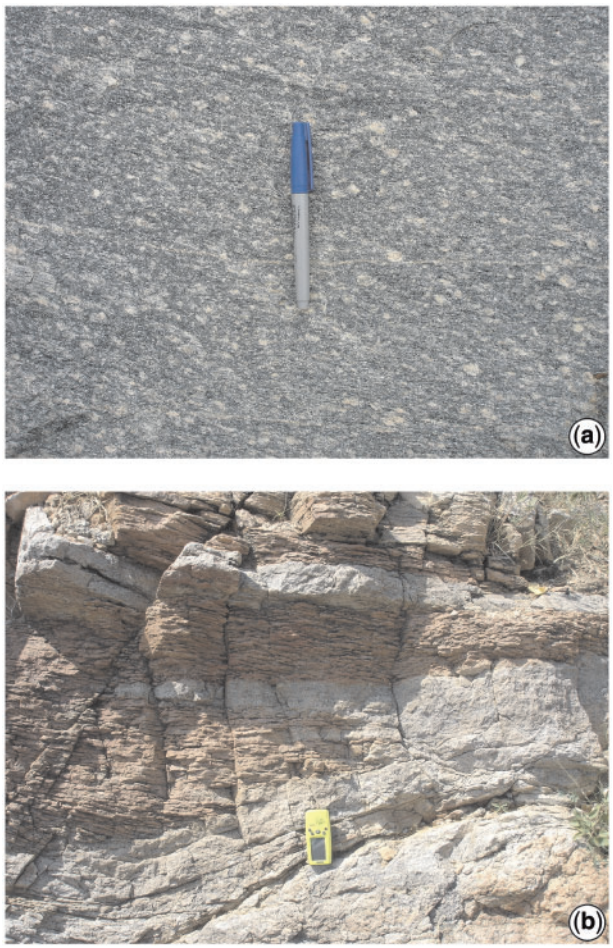

Fig. 3. Field photographs showing (a) pinkish grey original granite with pink K-feldspar phenocrysts in the Dosi pluton and (b) sharp contact between the microcline–albite granite (pink) and the albite granite (white) in the Dabla pluton. The length of pen is 13·5 cm, and that of the GPS is 9·5 cm.

<950 pg for Sr, levels that are insignificant for the analysed samples. Twenty measurements of the La Jolla Nd standard and 17 runs for the NBS 987 Sr standard, performed during this study, yielded a mean $^{143}Nd/^{144}Nd$ ratio of $0{\cdot}511854 \pm 7$ (2σ) and a mean $^{87}Sr/^{86}Sr$ ratio of $0{\cdot}710231 \pm 17$ (2σ) , respectively. Within-run precision (2σ mean) for $^{143}Nd/^{144}Nd$ and $^{87}Sr/^{86}Sr$ was $<10^{-5}$ and the external precision is also estimated at $<10^{-5}$. Values of $\varepsilon_{Nd(t)}$ were calculated for the zircon crystallization ages (t) and are based on the chondritic parameters of Jacobsen & Wasserburg (1980).

For oxygen isotope analysis, the coexisting minerals in the granites were separated by handpicking under a binocular microscope. Oxygen from ~1·5–2·5 mg whole-rock sample and ~1·0–1·6 mg mineral separates was extracted on a platinum sample holder in a F_2 atmosphere, using a CO_2 laser system for heating. The extracted gas was purified in a vacuum line and collected in a molecular sieve. The details of the method have been described by Sharp (1992). Purified O_2 gas was analysed directly on a Finnigan MAT 253 mass spectrometer at the University of Lausanne, Switzerland. Analyses of the whole-rock and mineral separates were monitored and corrected against the mean of three standard measurements. It should be noted that for the mineral separates, all mineral pairs of the same sample and all samples belonging to the same intrusion (except DS-11, which was measured with the Dabla samples) were measured during the same day to avoid additional uncertainties. For the whole-rock analyses, the Gore Mountain garnet standard ($\delta^{18}O = 5{\cdot}8‰$) was used for reference (Valley *et al.*, 1995), whereas for mineral separates the NBS-28 quartz standard ($\delta^{18}O = 9{\cdot}6‰$) was used. Standard statistics suggests an analytical uncertainty (1σ) of 0·23‰ for the whole-rock and 0·16‰ for the mineral separates. All oxygen isotope values are reported relative to VSMOW.

X-ray diffraction data were collected on a Philips PW1780 powder diffractometer with CuKα radiation at room temperature at the Mineralogisches Institut, University of Würzburg. The diffractometer is equipped with a secondary C (002) monochromator and a proportional counter. The lattice constants were refined with FULLPROF (Rodriguez-Carvajal, 2001) whereas, owing to the presence of additional phase(s), the atom positions could not be refined successfully. The reflections of the additional phase(s) were excluded from the refinement.

PETROGRAPHY AND MINERAL CHEMISTRY

Petrographic descriptions of the Biharipur and Dabla granites have been presented by Chaudhri *et al.* (2003) and Kaur *et al.* (2006). Here we give a full petrographic description of the Dosi granites for comparison with those of Biharipur and Dabla; representative mineral analyses of Dosi are given in the Supplementary Data Tables S1 and S2 (available for downloading at http://www.petrology.oxfordjournals.org). All the granite facies are characterized by marked differences between the abundances of albite and microcline.

We distinguish three important granite types, granite *sensu stricto* (hereafter referred to as 'original granite'), microcline–albite granite, and albite granite. Rocks referred to as 'microgranite' are finer-grained variants of the microcline–albite granite with the same mineralogical and chemical characteristics. 'Transitional granite' refers to a subordinate rock type in which the amount of microcline is intermediate between that of the microcline–albite granite and the albite granite. This rock type can be best distinguished in the normative Ab–Or–An plot (Fig. 4).

Original granite

The original granite is thought to be the only rock type that has not been affected by albitization. It is found in a few, relatively small outcrops and only at Dosi. It is a medium-grained (≤1 mm to 1·5 mm) foliated rock with a sparsely porphyritic texture. The major rock-forming phases (Table 1) are quartz (25–30% by volume), plagioclase (35–40%), K-feldspar (22–28%), amphibole and biotite (both 5–10%), accompanied by accessory titanite, zircon, allanite, apatite and magnetite with traces of secondary calcite. Quartz commonly occurs as elongated subhedral grains (Fig. 5a) of <1 mm in size (mostly in the range 0·2–0·7 mm). Locally, it also shows irregular margins and formation of subgrain boundaries, indicating the effect of solid-state deformation. Tabular to elongate K-feldspar (microcline with $Or_{93·5±0·5}$, $n = 16$; Supplementary Data Table S1) occurs as small (0·2–0·8 mm) crystals to occasional megacrysts (up to ~1 cm) with straight boundaries. The megacrysts show patchy-type perthite with blocks of albite (Fig. 5b), whereas the small microcline crystals are devoid of any perthitic intergrowth. The latter may be the product of recrystallization under subsolidus conditions. Occasional microcline islands in the plagioclase also indicate partial replacement of the mineral, presumably during the late magmatic evolution. The plagioclase occurs as equant, elongated, subhedral and fine- (0·2–0·7 mm) to medium-sized (1·0–1·5 mm) crystals. Albite and combined carlsbad–albite twinning is common, and plagioclase is oligoclase in composition with $An_{11·1–12·2}$ ($An_{11·6±0·4}$, $n = 17$; Supplementary Data Table S1), which suggests that this facies has not undergone albitization. Oriented dark green to bluish green, prismatic, interstitial amphibole imparts a lineation to the rock. It is potassian (with K = 0·25–0·49 a.p.f.u.; Leake *et al.*, 1997) ferropargasite ($Al^{VI} > Fe^{3+}$) (Fig. 6a and Supplementary Data Table S2; Leake *et al.*, 2004) and is iron-rich with X_{Fe} [= $Fe^t/(Fe^t + Mg)$] of 0·84–0·86. The amphibole is unaltered and is commonly interleaved with interstitial biotite. The latter is late magmatic in origin and formed, along with titanite, by replacement of amphibole. This is a typical feature of amphiboles in oxidized A-type granites (Dall'Agnol *et al.*, 1999). The biotite is an annite in composition (Fig. 6b and Supplementary Data Table S1) with X_{Fe} values between 0·71 and 0·74; that is, lower than those of the amphibole.

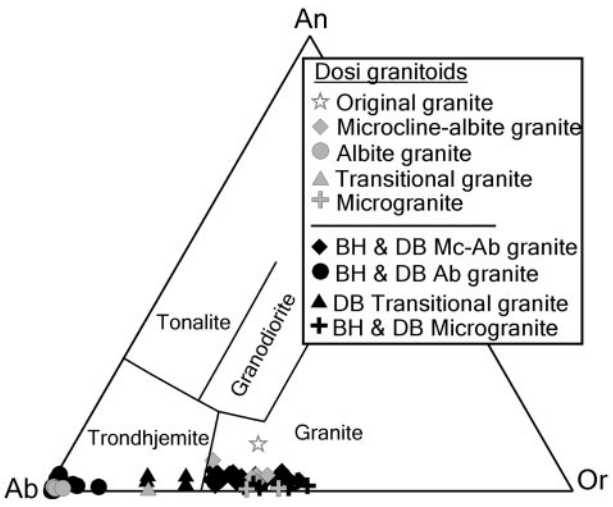

Fig. 4. Dosi granites in the ternary normative Ab–Or–An diagram (after Barker, 1979) along with the albitized granites of Biharipur and Dabla plutons. Data sources: Dabla, Chaudhri *et al.* (2003); Biharipur, Kaur *et al.* (2006). BH, Biharipur; DB, Dabla; Ab, albite; Mc, microcline.

Microcline–albite granite

The microcline–albite granite (Table 1) is distinguished from the original granite primarily by the complete

Table 1: Modal (vol. %) abundances for the A-type granite facies of the Dosi pluton, Rajasthan, NW India

Mineral	Original granite	Microcline-albite granite	Transitional granite	Albite granite	Microgranite
Quartz	25–30	30–35	32–36	30–35	30–35
K-feldspar	22–28	20–30	10–12	–	22–28
Oligoclase	35–40	–	–	–	–
Albite	–	35–40	50–55	60–65	35–40
Amphibole	5–10	5–10	<5	–	–
Biotite	5–10	<5–7	–	–	–
Accessory	Ttn, Zrn, Aln, Ap, Op, Cal	Ttn, Zrn, Aln, Ap, Op, Flt, Ep, Cal	Ttn, Zrn, Aln, Op, Flt, Ep, Cal	Flt, Cal, Zrn, Ttn, Op, Aln, Mc	Flt, Ttn, Chl, Zrn, Aln, Op, Cal

Aln, allanite; Ap, apatite; Cal, calcite; Chl, chlorite; Ep, epidote; Flt, fluorite; Mc, microcline; Op, opaque minerals; Ttn, titanite; Zrn, zircon.

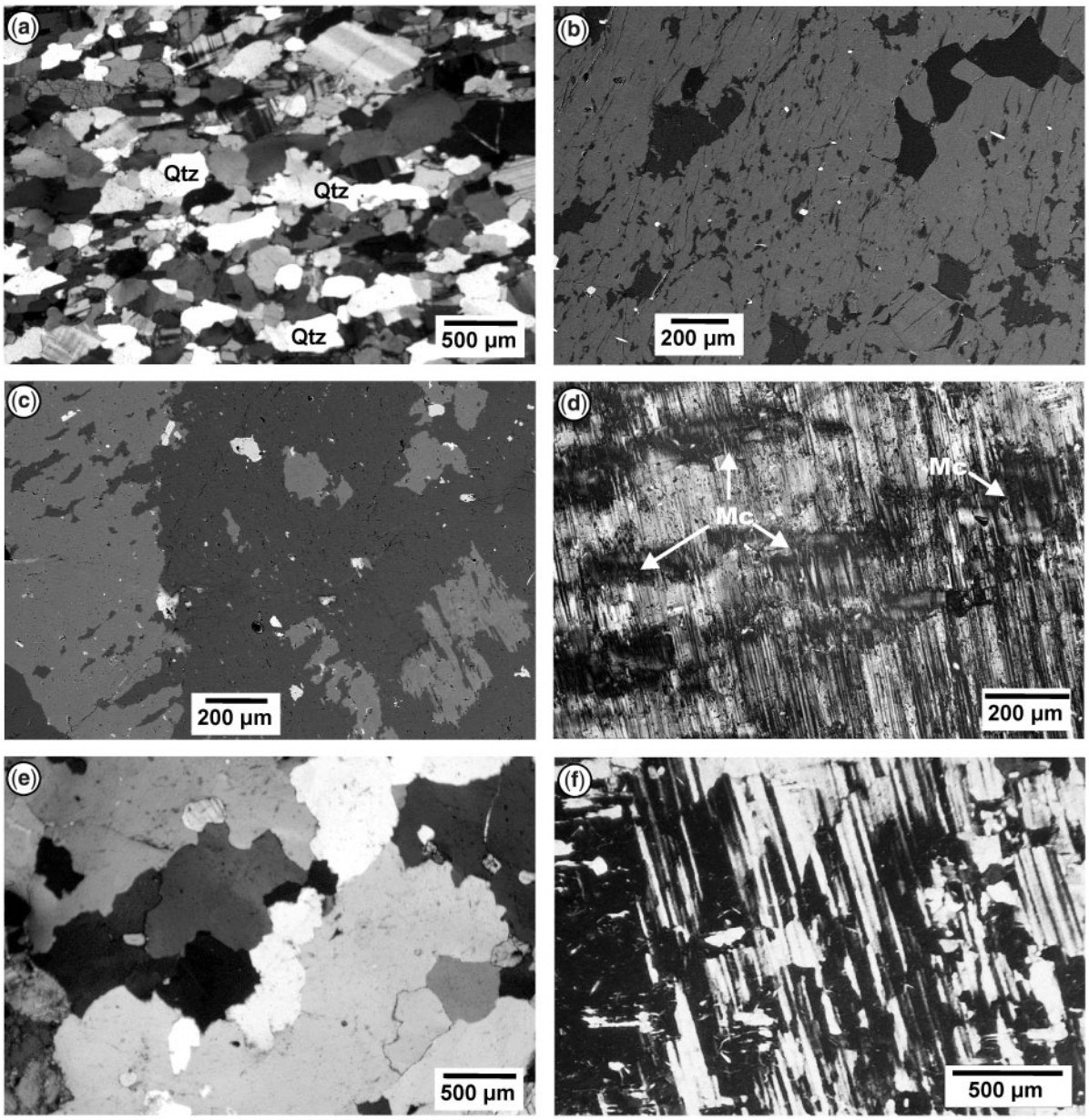

Fig. 5. Cross-polarized photomicrographs and SEM BSE images of Khetri A-type granites showing progressive albitization and silicification. (a) Original granite with elongated, interstitial, subhedral primary quartz. (b) Microcline (light grey) in the original granite showing patch-perthite (dark grey). (c) Similar microcline phenocryst (light grey) showing its partial albitization (dark grey area) in the microcline–albite granite. White spots are white mica. (d) More severe albitization of microcline results in the development of chessboard-type albite. Microcline remnants (Mc) show continuation of their twin lamellae with those of albite (microcline–albite granite). (e) A cluster of relatively large second generation quartz in the microcline–albite granite showing serrated grain boundaries. The white grain in the centre and the black to dark grey grain in the left are bulging into the neighbouring grains. (f) Chessboard-twinned albite without any traces of microcline in the albite granite.

replacement of oligoclase by albite, and the incipient replacement of microcline by albite. Here, all the felsic minerals show resorbed and diffuse grain boundary relationships, indicating alteration of these minerals (see Drummond *et al.*, 1986). The extent of albitization exhibited by microcline is variable from partial, patchy (Fig. 5c) to relic microcline enclosed in the chessboard-twinned albite (Fig. 5d); the albite produced in such cases is twinned as well as untwinned. Irrespective of the degree of albitization, the patches, blocks or remnants of microcline always show continuation of their twin lamellae with those of the newly formed albite (Fig. 5d; also see Kaur *et al.*, 2006,

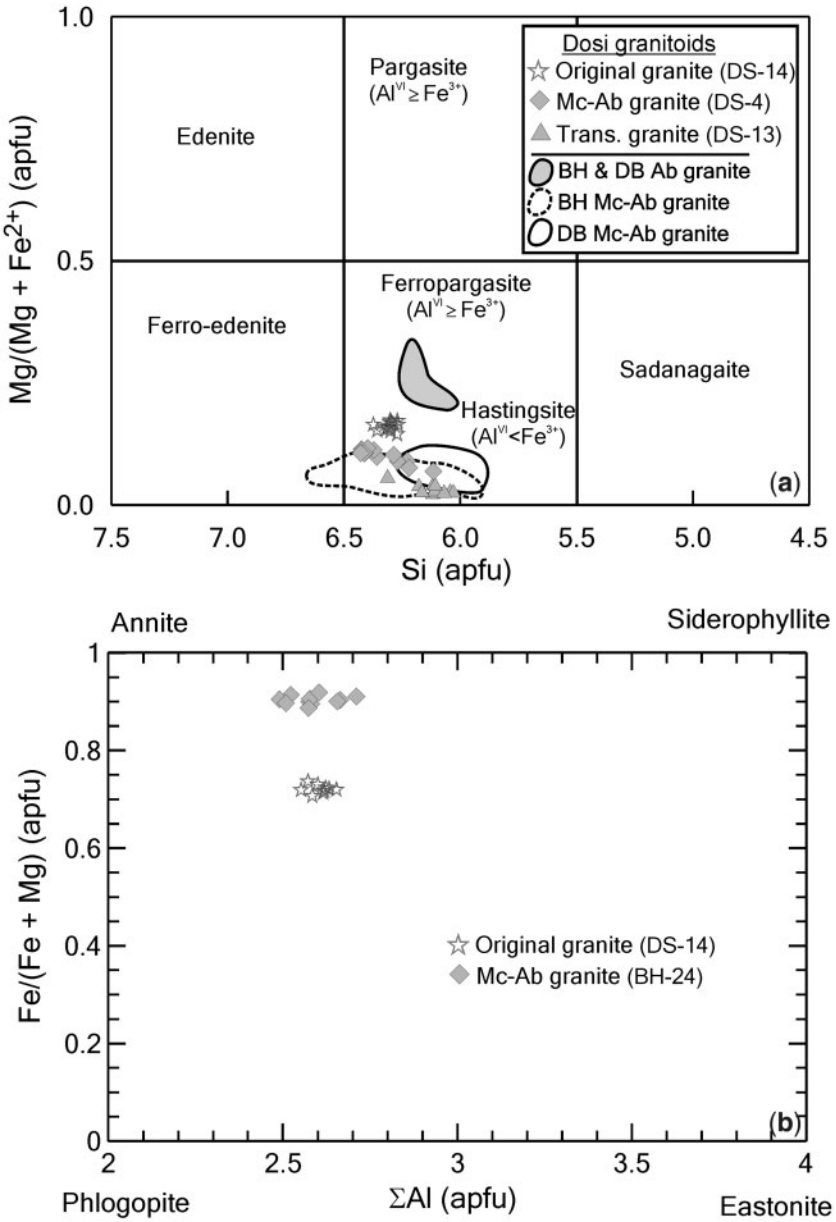

Fig. 6. Mineral compositions of Khetri A-type granites. (a) IMA classification (Leake *et al.*, 2004) of analysed amphiboles [$^{B}Ca \geq 1{\cdot}50$; $^{A}(Na + K) \geq 0{\cdot}50$; $Ti < 0{\cdot}50$]. (b) Classification of analysed biotite in the annite–sider ophyllite–eastonite–phlogopite quadrilateral. Explanation of abbreviations as given in Fig. 4.

fig. 3e). The composition of the microcline (20–30%) is the same as that in the original granite with $Or_{92{\cdot}4–95{\cdot}1}$ ($Or_{94{\cdot}1\pm0{\cdot}7}$, $n = 17$), and it is also similar to that in the Biharipur ($Or_{95{\cdot}1\pm0{\cdot}6}$, $n = 34$) and Dabla ($Or_{95{\cdot}2\pm0{\cdot}5}$, $n = 30$) microcline–albite granites. Equant to lath-shaped plagioclase is generally clouded, and moderately sericitized and epidotized. The plagioclase (35–40%) is virtually pure albite in composition, ranging from $An_{0{\cdot}5}$ to $An_{4{\cdot}4}$ ($An_{2{\cdot}0\pm1{\cdot}5}$, $n = 10$) similar to that found in Biharipur ($An_{1{\cdot}3\pm1{\cdot}0}$, $n = 33$) and Dabla ($An_{0{\cdot}8\pm0{\cdot}4}$, $n = 45$). Two generations of quartz (30–35%) are recognized in this granite. In addition to fine-grained primary quartz (0·4–1·0 mm), also observed in the original granite, relatively large quartz grains (2–3 mm) are also present. The latter type of quartz is always irregular and in places it shows serrated grain boundaries with crystals bulging into their neighbours (Fig. 5e). This suggests low-temperature grain boundary migration recrystallization (Passchier & Trouw, 2005). The large quartz crystals generally form clusters in the rock, and the largest are usually devoid of

subgrains (i.e. strain free). These features suggest that the relatively large quartz crystals formed as a result of either recrystallization or silica precipitation accompanying albitization. The occasional presence of miarolitic cavities with quartz crystals may also indicate silica precipitation in these rocks.

Amphibole (5–10%) is largely altered as evidenced by its association with epidote and calcite. In some of the Biharipur samples, calcite replaces amphibole in a pseudomorphic manner (Kaur *et al.*, 2006). Compared with the amphibole of the original granite, the mineral has been transformed to a potassic (with K >0·50 a.p.f.u.; Leake *et al.*, 1997) hastingsite ($Al^{VI} < Fe^{3+}$) (Fig. 6a) and shows higher values of X_{Fe} (0·88–0·93); the hastingsites of the Biharipur (X_{Fe} 0·93–0·95) and Dabla (X_{Fe} 0·91–0·97) counterparts have slightly higher X_{Fe} values. Nevertheless, the biotite, which occurs in these rocks as a minor or accessory phase (Table 1), preserves its annite composition (Fig. 6b) and, like amphibole, has higher X_{Fe} values of 0·90–0·91. Hedenbergite ($En_5Fs_{43}Wo_{47}$ to $En_9Fs_{47}Wo_{49}$; X_{Fe} 0·82–0·90; $n = 11$), which appears to be altering into andradite garnet ($Adr_{75·8–94·1}Grs_{2·4–18·8}Alm_{0·0–5·3}Sps_{0·4–1·1}$; $n = 8$), has also been observed in a single sample of the Dabla pluton. Interstitial fluorite is invariably present in these rocks, but is not observed in the original granite. Secondary hematite, epidote and calcite also occur in association with amphibole and albite. The primary accessory phases are similar to those in the original granite.

Albite granite

The albite granite is characterized by the almost complete absence of microcline, and in its extreme form it is essentially a quartz–albite assemblage (90–95% by volume) with variable, often small amounts of mafic minerals (Table 1). Exceptionally pure albite (60–65%) ranges from $An_{0·2}$ to $An_{0·6}$ ($An_{0·4±0·1}$, $n = 32$) in composition, identical to that of the Biharipur ($An_{0·5±0·3}$, $n = 20$) and Dabla ($An_{0·5±0·1}$, $n = 21$) albite granites. The most prominent feature of these rocks is the occurrence of chessboard-twinned albite (Fig. 5f), which is considered to have formed by the complete replacement of K-feldspar by albite (e.g. Anderson, 1937; Smith, 1974; Moore & Liou, 1979; Slaby, 1992). The occurrence of microcline relics in some albite crystals confirms this interpretation. The composition of such remnants of microcline ($Or_{95·1±1·0}$, $n = 10$) in the Biharipur albite granite is similar to that of the original and microcline–albite granites, suggesting that the composition of relic magmatic microcline has not been affected during albitization. This is in line with observations of Petersson & Eliasson (1997) for the albitized facies (episyenite) of the Bohus granite, Sweden.

In this rock, most of the quartz, which is similar in amount to that of the microcline–albite granite (Table 1), is relatively large (1–2 mm), irregular, strain-free and serrated of second-generation type. This implies that quartz was mainly recrystallizing at this stage of albitization. In Dosi no major mafic phases (amphibole and/or biotite) are present in the albite granite, whereas in Biharipur and Dabla actinolite is the main mafic mineral with minor biotite in these rocks. In the latter plutons, the actinolite crystals locally show remnants of potassic hastingsite, testifying to their transformation from the latter mineral. Such hastingsite relics (Fig. 6a) have lower X_{Fe} values (0·75–0·83) than those of the other facies. The X_{Fe} values of actinolite–magnesiohornblende amphiboles in Biharipur (X_{Fe} 0·32–0·64) and Dabla (X_{Fe} 0·39–0·67) albite granites are much lower compared with those of the original and microcline–albite granites. Titanite and allanite along with iron oxides, fluorite and secondary calcite occur as trace minerals in the Dosi albite granites.

Transitional granite

In this rock, oligoclase is completely replaced by usually clouded albite. Moreover, microcline shows a relatively advanced stage of albitization, its content being reduced to ~10 vol. % (Table 1). In Dosi, the composition of microcline ($Or_{93·0–94·8}$; $Or_{93·5±0·8}$, $n = 4$) is similar to that in the original and microcline–albite granites, and plagioclase is almost pure albite ($An_{0·2–1·6}$; $An_{1·1±0·4}$, $n = 10$). These feldspar compositions are also comparable to those in the transitional granite of Dabla [($Or_{96·0±1·4}$, $n = 10$) and ($An_{0·6±0·7}$, $n = 10$)]. Amphibole in this rock is potassic hastingsite (Fig. 6a), but with the highest X_{Fe} values among all the granite facies (X_{Fe} 0·97–0·98), whereas in the Dabla counterparts, the X_{Fe} values are slightly lower (X_{Fe} 0·91–0·93).

Microgranite

In Dosi, mafic minerals are negligible to absent in these rocks, comparable with the albite granite (Table 1). Interstitial fluorite is the most abundant accessory phase with some secondary chlorite. This facies contains amphibole as the main mafic mineral in Biharipur and Dabla. The microcline ($Or_{94·8±1·5}$, $n = 14$) and albite ($An_{0·7±0·3}$, $n = 17$) in Dosi and Biharipur ($Or_{96·1±0·57}$, $n = 10$) and ($An_{0·8±0·17}$, $n = 10$) are similar in composition, as observed for other facies. Amphibole in the Biharipur microgranite is largely potassic hastingsite with X_{Fe} values of 0·76–0·88. In places, the hastingsite has been altered to actinolite (X_{Fe} 0·52–0·57; Kaur *et al.*, 2006).

The occurrence of miarolitic cavities and the small grain size (<3 mm) of the major minerals in the Dosi pluton is consistent with emplacement of the magma at a relatively shallow crustal level, similar to the Biharipur and Dabla plutons (see Kaur *et al.*, 2006).

GEOCHEMISTRY

Bulk-rock chemical compositions of the Dosi granites are given in Table 2; chemical data for the Biharipur and

Table 2: Whole-rock chemical compositions for the Dosi granitoids, Rajasthan, NW India

	Original granite	Microcline–albite granite						Microgranite		Trans.	Albite granite		
Sample no.:	DS-14	DS-2	DS-4[1]	DS-5	DS-6	DS-18	DS-20	DS-8	DS-16	DS-13	DS-11	DS-15	DS-21
Lat. (°N):	28°03′	28°03′	28°03′	28°03′	28°03′	28°03′	28°04′	28°04′	28°03′	28°03′	28°03′	28°03′	28°04′
	17·6″	21·3″	30·9″	37·1″	35·4″	56·3″	0·9″	8·3″	59·8″	25·0″	46·8″	22·0″	8·2″
Long. (°E):	76°01′	76°01′	76°01′	76°01′	76°02′	76°01′	76°02′	76°02′	76°01′	76°02′	76°02′	76°01′	76°02′
	34·8″	48·0″	52·1″	45·4″	6·6″	58·1″	14·8″	25·2″	48·3″	18·3″	38·0″	32·4″	24·1″
SiO_2 (wt %)	71·2	74·7	73·9	73·9	75·7	76·3	73·1	77·4	76·4	78·6	78·6	79·8	79·1
TiO_2	0·47	0·25	0·27	0·27	0·21	0·17	0·31	0·07	0·08	0·15	0·13	0·11	0·09
Al_2O_3	13·12	12·21	12·28	12·16	11·99	11·49	13·50	12·03	11·89	11·85	12·24	12·20	12·35
$Fe_2O_3^t$	4·23	2·87	3·20	3·13	2·56	2·56	2·19	1·19	1·37	0·56	0·27	0·44	0·33
MnO	0·05	0·03	0·03	0·03	0·02	0·02	<0·01	<0·01	<0·01	<0·01	<0·01	<0·01	<0·01
MgO	0·53	0·18	0·18	0·16	0·13	0·08	0·46	0·03	0·03	<0·02	<0·02	<0·02	0·02
CaO	2·09	1·19	1·38	1·30	1·02	0·76	1·63	0·39	0·52	0·57	0·78	0·08	0·45
Na_2O	4·08	4·30	4·18	4·39	4·32	4·18	5·12	4·61	4·11	5·83	7·26	7·17	7·23
K_2O	3·74	4·00	4·27	3·96	4·08	3·91	3·18	4·03	4·63	1·97	0·09	0·14	0·29
P_2O_5	0·13	0·04	0·04	0·04	0·03	0·02	0·06	<0·01	0·01	0·05	0·01	<0·01	0·02
LOI	0·20	0·39	0·37	0·54	0·29	0·44	0·38	0·31	0·40	0·28	0·56	0·15	0·46
Sum	99·8	100·2	100·1	99·9	100·4	99·9	99·9	100·1	99·4	99·9	100·0	100·2	100·4
Cr (ppm)	<10	<10	<10	<10	<10	<10	<10	<10	<10	<10	<10	<10	<10
Co	27	28	34	28	35	37	28	29	32	25	31	25	22
Ni	<5	<5	<5	<5	<5	<5	<5	<5	<5	<5	<5	<5	<5
Zn	50	17	21	13	15	7	9	<5	<5	<5	<5	<5	<5
Ga	17	17	21	25	21	24	17	32	24	26	24	28	27
Rb	157	105	115	112	112	105	78	119	234	29	**1·02**	<5	<5
Sr	62	46	44	36	31	27	58	11	11	27	17	10	17
Y	94	93	124	137	142	170	58	124	140	177	121	48	128
Zr	331	340	383	404	327	371	213	219	225	368	274	256	305
Nb	27	24	36	31	35	40	15	45	50	40	36	24	58
Ba	515	620	575	554	466	396	327	92	98	297	22	35	50
Pb	13	<5	5	12	11	<5	<5	<5	<5	<5	<5	<5	<5
Th	34	33	35	36	36	44	23	45	43	35	44	37	53
U	5·2		6·4			6·8					2·9	2·4	
Hf	10·0		10·8			12·4		11·9			9·5	10·3	
Ta	2·1		2·4			2·8		5·4			3·3	4·4	
La	71·0		82·7			86·6		42·6			10·5	9·7	
Ce	133		159			172		80·3			21·4	17·1	
Pr	15·9		19·8			21·5		9·34			3·49	3·53	
Nd	62·3		78·7			84·9		33·2			19·3	17·8	
Sm	14·9		19·8			22·0		8·8			8·5	6·0	
Eu	2·08		2·21			1·98		0·51			1·01	0·54	
Gd	14·8		19·9			23·0		9·9			12·2	6·5	
Tb	2·6		3·7			4·5		2·3			2·8	1·4	
Dy	15·4		21·3			27·0		15·9			18·2	8·5	
Ho	3·1		4·3			5·7		3·7			3·9	1·7	
Er	9·6		13·2			18·0		13·1			12·6	5·2	
Tm	1·42		1·96			2·73		2·25			1·97	0·80	
Yb	8·4		11·5			15·9		13·9			11·7	4·4	
Lu	1·20		1·63			2·16		2·00			1·61	0·54	
∑REE	355·8		440·0			488·0		237·9			129·2	83·8	
$(La/Yb)_N$	5·7		4·9			3·7		2·1			0·6	1·5	
Eu/Eu*	0·43		0·34			0·27		0·17			0·30	0·26	
ASI	0·92	0·91	0·88	0·88	0·90	0·92	0·92	0·95	0·94	0·94	0·91	1·01	0·95
AI	0·82	0·93	0·94	0·55	0·96	0·97	0·88	0·99	0·99	0·99	0·98	0·98	0·99
10^4 Ga/Al	2·5	2·6	3·2	3·9	3·3	3·9	2·4	5·0	3·8	4·1	3·7	4·3	4·1
HPU	4·1		4·4			5·1					3·8	3·2	

$Eu/Eu^* = Eu_N/(Sm_N \times Gd_N)^{½}$. $HPU = D[0{\cdot}0967U\ (ppm) + 0{\cdot}0263Th\ (ppm) + 0{\cdot}035K\ (wt\ \%)]\ \mu W\,m^{-3}$ is heat production units (after Beardsmore & Cull, 2001), where D refers to density in $g\,cm^{-3}$ and is 2·69 for the original granite, 2·65 for the microcline–albite granite and the microgranite, and 2·62 for the albite granite and the transitional granite (Trans.). Bold Rb value is result from thermal ionization mass spectrometry (see Table 3).
[1]Data from Kaur *et al.* (2011*a*).

Dabla granites have been reported elsewhere (Chaudhri *et al.*, 2003; Kaur *et al.*, 2006).

The granites under consideration are all highly evolved with SiO_2 abundances greater than 70 wt %. The silica content increases from the original granite (71 wt %) through microcline–albite granite (73–76 wt %) to albite granite (79–80 wt %); in the transitional granites, the silica concentrations are close to those of the albite granite (Table 2). The abundance of Na_2O increases from ~4·0 wt % in the original granite to ~7·0 wt % in the albite granite, whereas K_2O decreases from ~4·0 wt % to ~0·2 wt %, implying a K–Na exchange. In the transitional granite, where microcline is present in minor amounts, the K_2O and Na_2O contents are about 2·0 wt % and 5·5 wt % respectively. In some albite granite samples of the Biharipur pluton, which have accessory microcline, the K_2O values vary between 0·6 and 1·0 wt %. The abundances of Rb and Ba are consistent with the K_2O depletion, and in some albite granites the Rb values are ≤1 ppm. Total Fe, Mg, Ca and Sr also decrease from the original granite to albite granite in the Dosi pluton (Table 2). The Biharipur and Dabla samples show no systematic variation in Mg, but Fe, Ca and Sr decrease from microcline–albite granite to albite granite (see Chaudhri *et al.*, 2003; Kaur *et al.*, 2006). Thorium concentrations range from 33 to 53 ppm in the Dosi granite, similar to the Dabla granite; they reach even higher values (up to 99 ppm) at Biharipur. Uranium concentrations are more variable and often low (relative to a 'normal' crustal Th/U ratio of about 4), ranging from 2·4 to 6·8 ppm, with lowest values occurring in the albite granites.

The REE patterns of the original granite and microcline–albite granite of the Dosi pluton are subparallel, moderately light REE (LREE) enriched [$(La/Yb)_N = 3·92–6·05$], and are characterized by nearly flat heavy REE (HREE) profiles (Fig. 7a). The microgranite exhibits a similar pattern, although having lower LREE abundances. The albite granite is depleted in LREE, whereas HREE profiles are parallel to those of the other granite types (Fig. 7a). All samples have prominent negative Eu anomalies ($Eu/Eu^* = 0·17–0·43$). The primitive-mantle-normalized trace element patterns of all granite facies in Dosi, Biharipur and Dabla are characterized by conspicuous negative anomalies for Sr, Ba, P and Ti (Fig. 7b and c); the original granite shows relatively less pronounced P and Ti minima. Overall, the multi-element patterns of all granite types are similar, except for the albite granites, which show prominent minima for Rb, Ba and K, and low LREE. All the granites are metaluminous, having aluminium saturation indices (ASI) ≤ 1 [molar $Al_2O_3/(CaO - 3·3P_2O_5 + Na_2O + K_2O)$] and agpaitic indices (AI) < 1 [molar $(Na_2O + K_2O)/Al_2O_3$]. The Fe-number [$Fe^* =$ wt % $FeO^t/(FeO^t + MgO)$] (Frost *et al.*, 200l; Frost & Frost, 2008) of the granites is high

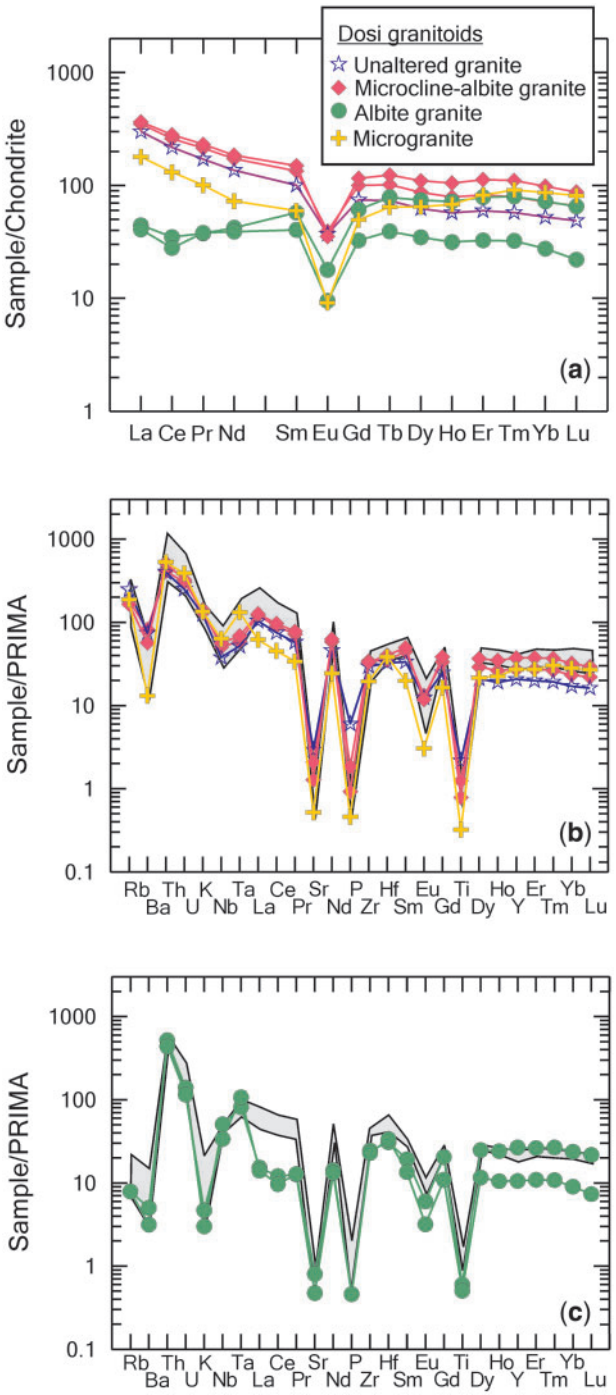

Fig. 7. (a) Chondrite-normalized REE abundance profiles for the Dosi granites. (b, c) Primitive mantle (PRIMA)-normalized multi-element patterns for the Dosi granites: (b) original granite, microcline–albite granite and microgranite; (c) albite granite. Normalizing values are after McDonough & Sun (1995). Shaded areas represent the fields of Biharipur–Dabla microcline–albite granite (b) and albite granite (c), and illustrate their similarity to the Dosi granite.

(ferroan) and increases with albitization from 0·88 (original granite) to 0·95 (albite granite). The Fe-rich nature of the ferromagnesian minerals, ferroan metaluminous character, high $10\,000 \times Ga/Al$ ratios (mostly >2·5), and elevated concentrations of Zr, Nb, Y and REE, as compared with I-, S- and M-type granites, suggest that the investigated rocks are typical A-type granites (Whalen *et al.*, 1987; Eby, 1990; Frost *et al.*, 2001).

The Sm–Nd and Rb–Sr whole-rock isotopic data are given in Table 3. The data are plotted as isochrons (ISOPLOT, Ludwig, 2003) in Fig. 8. The apparent Rb–Sr and Sm–Nd errorchron ages (1000 and 1460 Ma, respectively) are inconsistent with the crystallization ages (~1700 Ma) of the granites, presumably as a result of albitization (see discussion below).

Oxygen isotope data for the whole-rock and mineral fractions are given in Table 4. The whole-rock $\delta^{18}O$ values show a systematic increase (Fig. 9a) from the original granite (7·1‰) to the albite granite (8·7–9·9‰). Various mineral separates also display a similar increase in $\delta^{18}O$ values (Table 4). The $\delta^{18}O$ values of quartz are higher than those of feldspar and whole-rock values. In addition, the $\delta^{18}O$ quartz values are higher in albite granites than in the less altered rocks by 1–2‰. The feldspars and whole-rock $\delta^{18}O$ values are similar, as feldspars are the dominant phases in these granites. Nearly all the granites have $\Delta Qtz–Fsp/Ab$ of around 2‰, except for sample DB-33 and to a lesser extent DS-4 (Table 4). There is an enrichment in SiO_2 concentration with increasing $\delta^{18}O$ quartz and whole-rock values (Table 4, Fig. 9b).

Table 3: Nd and Sr isotopic systematics for the A-type granites, Rajasthan, NW India

Sample	Rock type	Sm (ppm)	Nd (ppm)	$^{147}Sm/^{144}Nd$*	$^{143}Nd/^{144}Nd$†	$\varepsilon_{Nd(t)}$‡	T_{DM}§ (Ga)	Rb (ppm)	Sr (ppm)	$^{87}Rb/^{86}Sr$	$^{87}Sr/^{86}Sr$
Biharipur pluton											
BH-18	Mc–Ab granite	22·38	96·75	0·13983	0·511884 ± 13	−2·3	2·28	104·88	19·11	16·2879	0·974046 ± 14
BH-34	Mc–Ab granite	18·60	78·68	0·14289	0·511985 ± 8	−1·0	2·18	140·96	12·08	35·5229	1·241378 ± 12
BH-58¶	Mc–Ab granite	19·18	82·51	0·14054	0·511961 ± 8	−1·0	2·18	80·59	18·98	12·5190	0·902056 ± 12
BH-8¶	Ab granite	13·07	56·54	0·13974	0·511880 ± 6	−2·4	2·29	15·23	12·73	3·4785	0·762916 ± 15
BH-65	Ab granite	19·89	115·41	0·10414	0·511512 ± 8	−1·8	2·24	1·55	4·59	0·9829	0·757383 ± 14
BH-3	Microgranite	16·78	72·95	0·13904	0·511939 ± 8	−1·1	2·19	198·81	4·35	170·132	3·631219 ± 23
BH-30¶	Microgranite	25·84	112·30	0·13913	0·511865 ± 14	−2·6	2·30	110·48	22·03	14·8959	0·981963 ± 17
Dabla pluton											
DB-11¶	Mc–Ab granite	18·07	76·75	0·14231	0·511913 ± 12	−2·3	2·28	89·55	26·82	9·7894	0·844901 ± 9
DB-33¶	Mc–Ab granite	18·86	91·93	0·12399	0·511778 ± 7	−0·9	2·17	90·87	16·36	16·3752	0·902506 ± 7
DB-36	Mc–Ab granite	16·94	75·58	0·13546	0·511878 ± 8	−1·5	2·22	110·84	27·75	11·7417	0·871501 ± 12
DB-30¶	Ab granite	12·48	44·15	0·17081	0·512207 ± 6	−2·8	2·32	1·13	11·43	0·2875	0·734718 ± 14
DB-37	Ab granite	12·58	42·49	0·17891	0·512218 ± 7	−4·4	2·43	0·82	8·44	0·2803	0·741196 ± 16
DB-16	Microgranite	6·52	31·98	0·12321	0·511766 ± 10	−1·0	2·18	102·11	9·83	31·0057	1·036588 ± 11
Dosi pluton											
DS-14**	Original granite	15·59	69·31	0·13594	0·511840 ± 7	−2·3	2·28	163·66	60·73	7·9398	0·895842 ± 10
DS-4**	Mc–Ab granite	20·06	85·15	0·14240	0·511964 ± 8	−1·3	2·20	117·80	39·80	8·6965	0·868702 ± 7
DS-11	Ab granite	8·29	19·34	0·25928	0·513015 ± 8	−6·3	2·59	1·02	8·71	0·3400	0·745046 ± 14
DS-8	Microgranite	8·89	36·04	0·14916	0·512070 ± 7	−0·7	2·16	122·91	7·14	53·200	1·409777 ± 15
BCR2 standard (Split 1161)											
BCR2		6·55	28·60		0·512650 ± 9			46·41	336·76		0·704959 ± 7
BCR2-1		6·57	28·69		0·512651 ± 6			47·10	338·47		0·704990 ± 12
BCR2-2		6·57	28·70		0·512648 ± 8			47·08	339·40		0·705044 ± 8

*Estimated error for $^{147}Sm/^{144}Nd$ is less than 0·5%.
†$^{143}Nd/^{144}Nd$ normalized to $^{146}Nd/^{144}Nd = 0·7219$; within-run error expressed as 2σ in the least significant digits.
‡Initial ε_{Nd} values calculated using the present-day values of $(^{143}Nd/^{144}Nd) = 0·512638$ and $(^{147}Sm/^{144}Nd) = 0·1966$ for the chondritic uniform reservoir (Jacobsen & Wasserburg, 1980), and the crystallization age of 1700 Ma.
§Depleted mantle model ages calculated using the two-stage model of Liew & Hofmann (1988).
¶Nd data from Kaur *et al.* (2007).
**Data from Kaur *et al.* (2011*a*).
Mc, microcline; Ab, albite.

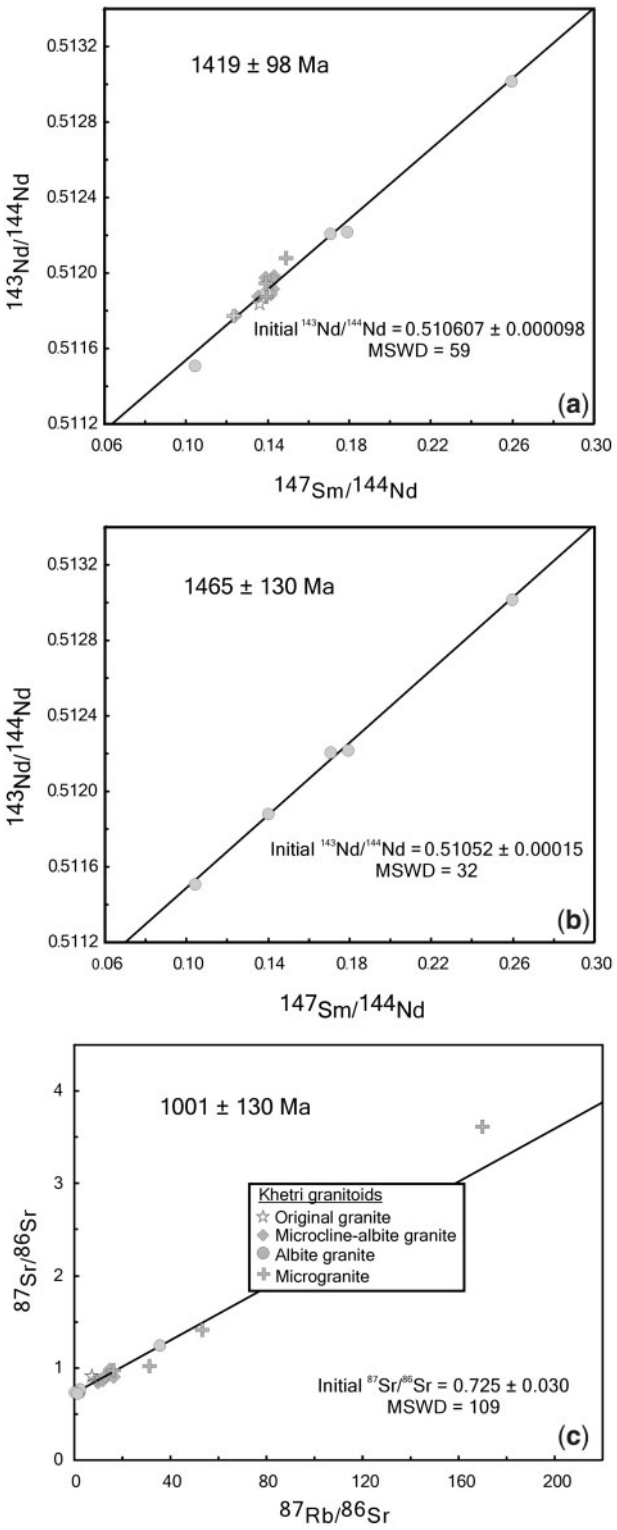

Fig. 8. Nd–Sr isotope data for samples from Dosi, Dabla and Biharipur granites in (a) Sm–Nd isochron-type diagram for all the analysed original and albitized granites, (b) Sm–Nd diagram for the completely albitized granites and (c) Rb–Sr isochron diagram. None of these diagrams represents a true isochron because of excessive scatter. The possible age significance is discussed in the text.

DISCUSSION

Constraints on the albitization process

On the basis of petrographic evidence, we infer that the 'original' granite at Dosi is closest to the primary magmatic granite. Both spatial and chemical relationships in the microcline–albite granite, where oligoclase has been completely replaced by albite, are consistent with the interpretation that this rock type represents the first stage (= leading front) of albitization. In the albite granite, microcline has also been completely replaced by albite, leading us to the conclusion that this represents the final, most advanced stage of albitization (equivalent to the second, trailing metasomatic front). The albitized intrusive rocks (Dosi–Biharipur–Dabla) occur along the same strike continuation; these are of similar age with similar outcrop patterns (Fig. 2) and chemical compositions (Fig. 7). In view of this and the sparse occurrence of outcrops of the original granite, we assume that the protolith for all the granites was fundamentally similar. In the following, we discuss evidence that helps to constrain the two stages of albitization in the Khetri A-type granites.

Field relations

The microcline–albite granite and albite granite can be readily distinguished as the former is mostly pink and the latter is always white in colour. The albite granite facies in the Dosi pluton is largely confined to the outer margin and albitization in the other plutons has also generally progressed from the margin inward. Whitening of feldspars or granitoid outcrops is one of the notable megascopic indicators for strong and pervasive albitization and has commonly been observed in many albitized granitoids (e.g. Baker, 1985; Charoy & Pollard, 1989; Petersson & Eliasson, 1997).

The lack of any crosscutting relationships between the microcline–albite granite and the albite granite, along with the presence of enclaves or tongues of both rock types within one another (Fig. 2), suggests that these two facies were originally synchronous (see Chaudhri *et al.*, 2003). This interpretation is in accord with the identical, but imprecise U–Pb zircon crystallization ages of the microcline–albite granite (1662 ± 33 Ma) and the albite granite (1662 ± 31 Ma) from the Biharipur pluton (Kaur *et al.*, 2007). At the contact, the microcline–albite granite shows a strong foliation, whereas the albite granite is only weakly foliated (Fig. 3b). This may be partly caused by the near-absence or lower amounts of ferromagnesian minerals in the latter, and by the presence of newly crystallized and/or recrystallized, relatively coarse-grained and unstrained quartz. This observation also indicates that the albitization took place subsequent to the earlier deformation that generated the foliation of the original granite. All observed contacts of the albite granite are with microcline–albite granite, not with the original granite. This is

Table 4: Oxygen isotope data ($\delta^{18}O$ ‰ relative to VSMOW) of whole-rock (WR) and mineral separates for the A-type granites, Rajasthan, NW India

Sample	Rock type	WR	Qtz	Fsp	Ab	Am + Bt (wt %)	Am	Bt	$\Delta_{Qtz-Ab/Fsp}$	$T°_{Qtz-Ab}$*	$T°_{Qtz-Ab}$†	SiO_2
Biharipur pluton												
BH-34	Mc–Ab granite	7·95	9·09	7·20				2·40	1·89	385	416	75·8
BH-65	Ab granite	9·32	10·42		8·56		6·48		1·86	392	421	79·4
Dabla pluton												
DB-33	Mc–Ab granite	8·46	9·48	8·55			6·50		0·93	751	732	73·8
DB-37	Ab granite	9·85	11·65		9·37		7·62		2·28	306	348	76·5
Dosi pluton												
DS-14	Original granite	7·14	8·98	6·67		3·67			2·31			71·2
DS-4	Mc–Ab granite	7·51	8·88	7·40			4·28		1·48	500	513	73·9
DS-13	Trans. granite	7·55	8·96	6·89					2·07	345	382	78·6
DS-11	Ab granite	8·70	10·16		8·24				1·92	378	409	78·6

*Apparent temperatures after Zheng (1993).
†Apparent temperatures after Clayton & Keiffer (1991).
Ab, albite; Am, amphibole (ferropargasite: DS-14; hastingsite: DB-33 and DS-4; actinolite: BH-65 and DB-37); Bt, biotite; Fsp, feldspar (microcline + albite, microcline + oligoclase: DS-14), Mc, microcline. Trans., Transitional.

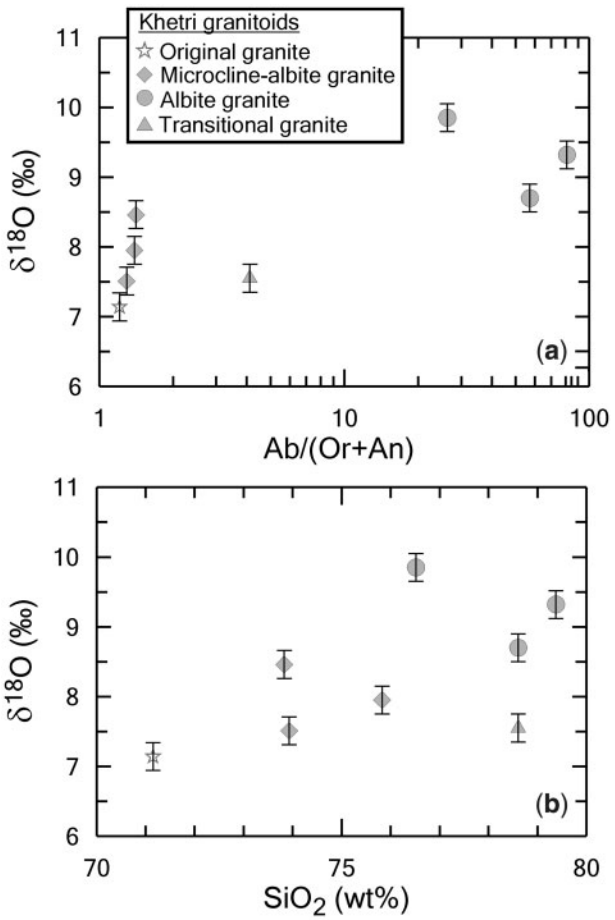

Fig. 9. Whole-rock $\delta^{18}O$ values against (a) an index of albitization, the normative Ab/(Or + An), showing increasing values during progressive albitization and (b) SiO_2 (wt %) also showing a systematic increase with advancing silicification. Error bars in both the diagrams are at 0·2‰.

consistent with the two-stage metasomatic replacement model outlined below.

Geochemical changes during albitization

The main major element changes are illustrated in the normative Ab–Or–An diagram, where the rocks are delineated by their variable contents of albite as compared with the other feldspar components (Fig. 4). The original granite and the microcline–albite granites occupy the granite field, and the former plots more towards the An corner. Whereas the transitional granites plot more towards the Ab corner, the albite granites occupy the extreme Ab corner in the trondhjemite field. The decrease in Rb abundances from ~160 ppm to ~1 ppm (Fig. 10) is also compatible with progressive albitization of K-feldspar and loss of mafic phases, because Rb is rather compatible in K-feldspar, potassic hastingsite and biotite but highly incompatible in albite.

To quantify relative losses, gains or immobility of elements in a metasomatic event, the whole-rock data are subjected to isocon analysis (Fig. 11), where concentrations of elements in the altered rock are plotted against those in the original rock, and a reference line corresponding to a zero concentration change (an isocon) intersects the axes at the origin of the plot (Grant, 1986, 2005). Elements that remain immobile during alteration should plot on, and thus define, the isocon, whereas those that have experienced gains or losses relative to their concentration in the original rock will plot above or below the isocon, respectively. The slope of the isocon may be based on the constant concentration of some component, constant mass or constant volume (Grant, 1986).

The massive loss of K and gain of Na, and probably also the formation of new coarser quartz in the albitized

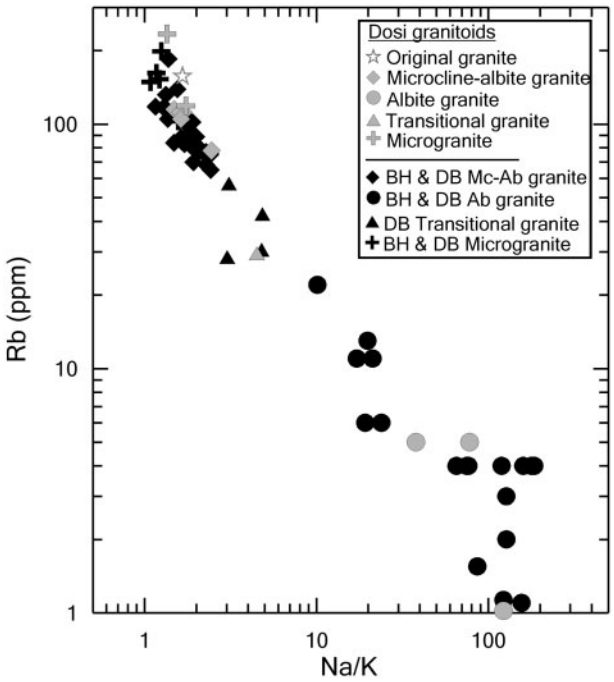

Fig. 10. Rb (ppm) vs Na/K (cationic) showing the progressive depletion of Rb with the advancing albitization of K-feldspar. Data sources and explanation of abbreviations are the same as in Fig. 4.

granites (see above) suggest that albitization is accompanied by significant mass and volume change. The whole-rock major and trace element data have been analysed (see Supplementary Data Tables S3 and S4) using an approach similar to that shown in table 1 of Grant (2005). Assuming that the precursor to all the albitized rocks under consideration had a constant chemical composition, isocon diagrams with a best fit of the data forming a linear array through the origin are constructed (Grant, 2005; Fig. 11).

Figure 11a and b shows the apparent gains and losses during the first stage of albitization, the formation of microcline–albite granite (average of samples DS-2, DS-4, DS-5, DS-6, DS-18 and DS-20) from the original granite (sample DS-14). Figure 11a shows two tentative isocons, one passing through Al and the other through Na, Nb and U. These are intended to show the limiting envelope of possible isocons. Above this envelope is H [for loss on ignition (LOI) or H_2O] indicating hydration at this stage of albitization, which is petrographically expressed as sericitization and epidotization. Although the absolute amount of sericite and epidote are minor (LOI <0·5 wt %), the relative change in H_2O between the original and the metasomatized samples is relatively large. Below this envelope are Fe, Ca, Ti, Mg, Mn, P, Rb, Sr and Zn, indicating loss of these elements. Considering the common immobility of Al during such a metasomatic event (Grant, 1986), we prefer to use the isocon through Al for the following discussion. In this case, Si shows a slight gain, mostly as a result of secondary quartz precipitation. Also, the transformation of oligoclase to albite is insufficient to cause a drastic change in bulk-rock Na_2O. However, some trace elements, such as Y, Zr, Nb and the REE, do show apparent gains. Nevertheless, this isocon diagram must be interpreted with considerable caution, because we have little information on the initial homogeneity of the granite body with respect to trace elements. Thus, the apparent incompatible element enrichment is most probably due to concentration increases in the residual liquid during fractional crystallization. It is therefore unlikely that any of these apparent 'gains' can be ascribed to the metasomatic albitization process. On the other hand, the apparent losses of Rb, Sr, Fe, Zn, Ca, Mg, P and Ti are likely to be primarily or partly caused by the albitization process.

The gains and losses during the second and final stage of the metasomatic change to form the pure albite granite (average of samples DS-11, DS-15 and DS-21), shown in Figures 11c and d, are much more clear-cut. Assuming an isocon through Al, there is a significant gain in Na and a slight gain in Si. Some of the apparent gains of relatively immobile incompatible trace elements (Th, Nb, and Ga) are again unlikely to be related to the metasomatic process. In contrast, there are now very large losses of Rb, Ba, Sr, LREE, Zn and U, in addition to the continued losses of the major elements K, Mg, Fe, Ca, P and Ti. The loss of Rb is more substantial than that of Sr; Ca and Sr show similar losses, as do K and Rb (Fig. 11d). Most of these losses can be directly related to the dissolution of mafic phases and the replacement of microcline by albite. The consistent loss of LREE (but, with one exception, not HREE) is not so easily explained by the changes in the major phases. The LREE are rather incompatible in both K-feldspar and albite. Loss of apatite, which is probably responsible for the decrease in P_2O_5, may also account for some of the observed LREE/HREE fractionation. However, this mineral is a good host for LREE in peraluminous and peralkaline granitoids, but less so in metaluminous granitoids (Bea, 1996). Therefore, allanite may be a better candidate than apatite to account for the loss of LREE. Allanite has very high partition coefficients for the LREE, ranging from about 200 in granodioritic systems (Hermann, 2002) to 3000 in high-silica rhyolites (Mahood & Hildreth, 1983); it also has moderately high partition coefficients for Th, and relatively low coefficients for the HREE and Y (Mahood & Hildreth, 1983; Hermann, 2002). Thus allanite probably contains most of the LREE budget of the whole-rock. Dissolution of a significant portion, but not all, of the allanite along with apatite may thus have reduced the LREE of the Dosi albite granites without strongly affecting the HREE and Th.

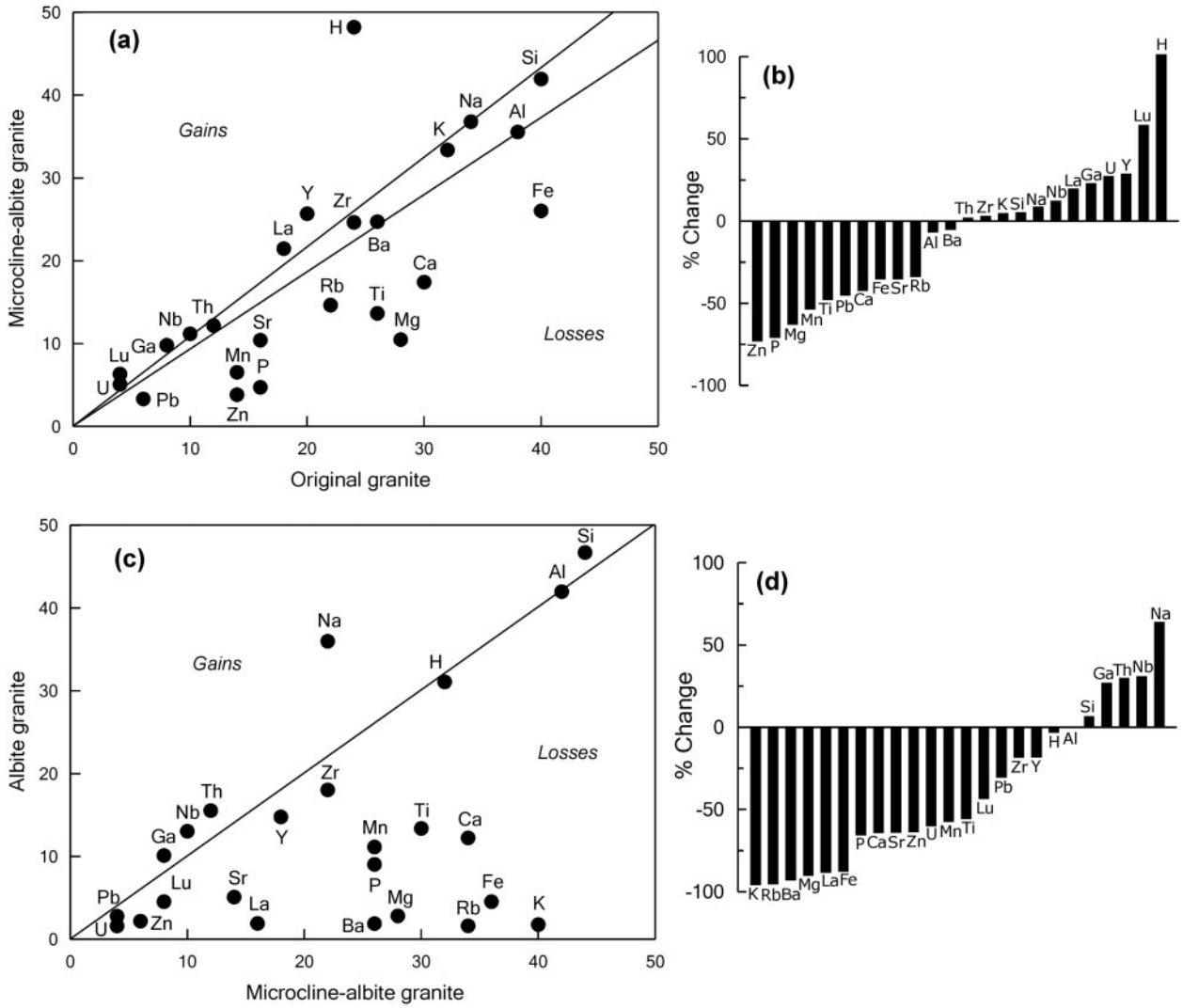

Fig. 11. Isocon plots (after Grant, 2005) to assess whole-rock chemical changes for (a) the microcline–albite granite (average of samples DS-2, DS-4, DS-5, DS-6, DS-18 and DS-20) and (c) the albite granite (average of samples DS-11, DS-15 and DS-21), representing the initial and final stages of albitization, respectively. (b) and (d) show the same data as per cent changes relative to the original granite and the microcline–albite granite, respectively. Major element data are in wt % and trace elements in ppm, and labels for major oxides are abbreviated to the cation elements. Data above the isocon refer to elements apparently enriched during albitization. Data below the isocon represent elements lost during albitization, with the most extreme depletion seen in the completely albitized granites.

In summary, because the starting compositions of the metasomatized rocks are likely to be somewhat variable as a consequence of variable fractional crystallization, the isocon analysis of the first stage (Fig. 11a and b) yields somewhat ambiguous results. In contrast, the final stage of albitization (Fig. 11c and d) shows unambiguous and large losses of K, Rb, Ba, Fe, Mg, Ca, Sr, P and Ti.

Mineralogical constraints

Complete replacement of K-feldspar by albite has been ascribed to a mechanism of alkali ion exchange between fluid and feldspar phases (Orville, 1963) by a replacement reaction (Moore & Liou, 1979):

$$KAlSi_3O_8^{solid} + (Na^+)_{aq} \Leftrightarrow NaAlSi_3O_8^{solid} + (K^+)_{aq}. \quad (1)$$

The microcline (average range, $Or_{93\cdot5}$–$Or_{96\cdot0}$) in the albitized granites has a composition similar to that in the original granite ($Or_{92\cdot5}$–$Or_{94\cdot3}$), suggesting that the pre-existing microcline is converted directly to albite. In contrast, the composition of plagioclase in the albitized granites, where the mineral is virtually pure albite, is strikingly different from the oligoclase in the original granite. This is true for all the plagioclase; that is, albite formed from albitization of microcline has the same

composition as albite formed from magmatic plagioclase. Following Engvik *et al.* (2008) and Hövelmann *et al.* (2010), the transition from oligoclase to albite can be formulated by a simplified, allochemical and Al-conservative reaction:

$$\underset{\text{oligoclase An}_{12}}{Na_{0\cdot88}Ca_{0\cdot12}[Al_{1\cdot12}Si_{2\cdot88}O_8]} + 0\cdot24(Na^+)_{aq} + 0\cdot48\ H_4SiO_4 = \underset{\text{albite An}_0}{1\cdot12\ Na[AlSi_3O_8]} + 0\cdot12\ (Ca^{2+})_{aq} + 0\cdot96\ H_2O. \quad (2)$$

Because the whole-rock Al concentrations are fairly constant (see Table 2), we regard this reaction as more likely than the alternative, constant-volume and Al-producing reaction also proposed (and preferred) by those researchers. The Ca^{2+} liberated in the reaction might have been fixed by calcite, epidote and fluorite.

The absence of intermediate plagioclase compositions between An_2 and An_{12} is consistent with the solubility gap (peristerite gap) that forms at temperatures between about 525 and 400°C (Moody *et al.*, 1985). It confirms the low-temperature nature of the albitization process. It also implies that plagioclase (An_{12}) in the original granite has preserved its magmatic composition, because the peristerite gap extends from about An_2 to An_{20} (Moody *et al.*, 1985), and this would not allow formation of An_{12} by partial albitization at low temperatures.

The preservation of both morphology and crystal structure during the transformation of microcline and oligoclase to albite implies re-equilibration of these mineral phases in the presence of a fluid by an interface-coupled dissolution–reprecipitation mechanism (Putnis & Putnis, 2007; Niedermeier *et al.*, 2009; Hövelmann *et al.*, 2010). This mechanism also suggests that the incomplete conversion of microcline to albite in some of the albitized granites may be because porosity was not generated in the newly formed albite, which stopped the transformation reaction.

During progressive albitization, Ti and Mn show a systematic decrease in amphiboles, whereas Fe increases relative to Mg (X_{Fe} from 0·84 in potassian ferropargasite to ~0·95 in potassic hastingsite; Supplementary Data Table S2 and Fig. 6a) during the first stage of albitization, and ultimately decreases while Mg increases (X_{Fe} ~0·40; see Kaur *et al.*, 2006, table 3) in the second stage of albitization (formation of actinolite–magnesiohornblende). The loss of these elements is manifested by local magnetite deposits in some of the albitized granites (e.g. Dhanota), as well as magnetite-rich bands along the margins of these granites. The main oxide phase, magnetite, is also invariably altered to hematite in the albitized granites (Kaur *et al.*, 2006). Although biotite has preserved its composition (annite) in the albitized granites, its X_{Fe} value increases and its amount decreases from the original granite to the microcline–albite granite (Fig. 6b).

The transformation of potassian ferropargasite in the original granite (e.g. sample DS-14) to form potassic hastingsite in the microcline–albite granite (e.g. sample DS-4) can be formulated by the following simplified, allochemical and Al-conservative reaction:

$$\underset{\text{potassian ferropargasite}}{K_{0\cdot5}Na_{0\cdot6}Ca_{1\cdot9}Mg_{0\cdot7}Fe^{2+}_{3\cdot6}Fe^{3+}_{0\cdot2}Ti_{0\cdot1}Al^{VI}_{0\cdot4}[(OH)_2Al^{IV}_{1\cdot7}Si_{6\cdot3}O_{22}]} + 0\cdot6H_4SiO_4 + 0\cdot1\ K^+ + 0\cdot1\ Na^+ + 0\cdot4\ Fe^{3+} = \underset{\text{potassic hastingsite}}{K_{0\cdot6}Na_{0\cdot5}Ca_{1\cdot9}Mg_{0\cdot4}Fe^{2+}_{3\cdot6}Fe^{3+}_{0\cdot6}Ti_{0\cdot1}Al^{VI}_{0\cdot2}[(OH)_2Al^{IV}_{1\cdot7}Si_{6\cdot3}O_{22}]} + 0\cdot2\underset{\text{albite}}{Na[AlSi_3O_8]} + 0\cdot3Mg^{2+} + 0\cdot8H_2O + 0\cdot8\ H^+. \quad (3)$$

An analogous reaction may have taken place for the decomposition of potassic hastingsite to form actinolite in the course of extreme albitization. As ferromagnesian silicate phases are virtually absent in the albite granites of the Dosi pluton, we use albite granite BH-8 from the Biharipur pluton as an example (data from Kaur *et al.*, 2006), where remnants of potassic hastingsite in the actinolite suggest that hastingsite decomposed to form actinolite + albite + hematite according to the following reaction:

$$\underset{\text{potassic hastingsite}}{K_{0\cdot6}Na_{0\cdot4}Ca_{1\cdot9}Mg_{1\cdot0}Fe^{2+}_{3\cdot0}Fe^{3+}_{1\cdot0}[(OH)_2Al_{1\cdot8}Si_{6\cdot2}O_{22}]} + 6\cdot8H_4SiO_4 + 1\cdot3Na^+ + 0\cdot1Ca^{2+} + 1\cdot9Mg^{2+} = \underset{\text{actinolite}}{Ca_{2\cdot0}Mg_{2\cdot9}Fe^{2+}_{2\cdot0}Fe^{3+}_{0\cdot1}[(OH)_2Al_{0\cdot1}Si_{7\cdot9}O_{22}]} + 1\cdot7\underset{\text{albite}}{Na[AlSi_3O_8]} + 0\cdot9\underset{\text{hematite}}{Fe_2O_3} + 0\cdot6\ K^+ + 10\cdot9\ H_2O + 5\cdot4\ H^+ + 0\cdot1\ Fe^{2+}. \quad (4)$$

To balance these reactions, some additional Si must have been supplied, together with Na, to form albite. In reaction (4), the Al released during the transformation of amphibole is used to form the additional albite. In reaction (3) some Fe is used and Mg released, whereas Fe is liberated in reaction (4) where it may form an iron oxide mineral (e.g. hematite and/or magnetite) or be removed from the system. The whole-rock compositions and isocon diagrams discussed above show that, during the advanced stages of metasomatic alteration, Si was gained together with Na, whereas K, Mg and Fe were lost from the bulk rock. Therefore, the Mg necessary to transform potassic hastingsite into actinolite according to equation (4) must have been supplied only at a local scale.

The above considerations suggest that during the first stage of albitization, the Si gain is probably linked to the crystallization of new quartz. During the subsequent stage

of albitization, the Si gain is mainly related to the crystallization of a more Si-rich amphibole (actinolite) and additional albite [reaction (4)]. The crystallization of new quartz does not seem to play any significant role in Si gain at this stage as its modal abundance in the microcline–albite granite and albite granite remains more or less the same (Table 1).

Isotopic relationships

With exception of the Biharipur samples, the albite granites have higher $^{147}Sm/^{144}Nd$ than the original and microcline–albite granites (Table 3). In contrast, the microcline–albite granites show little variation in $^{147}Sm/^{144}Nd$ and initial ε_{Nd} values, and they therefore yield reasonably consistent crustal residence ages (about 2·2 Ga). All the measured samples from the three plutons, spanning a distance of about 25 km, yield a Sm–Nd errorchron age of 1419 ± 98 Ma (Fig. 8a). A separate plot for the completely albitized granites (Fig. 8b) shows a similar age (1465 ± 130 Ma) because the slopes of both errorchrons are governed by the albite granites. Although these isochrons are clearly disturbed (as indicated by high MSWD values), the apparent age of about 1460 Ma might provide an age estimation for the albitization, at least to the extent that it occurred substantially later than the magmatic emplacement of the granites.

The large scatter seen in the Rb–Sr isochron plot (Fig. 8c) is not surprising in view of the high mobility of both Sr and Rb during albitization. Therefore, the apparent age of *c.* 1000 Ma may have no geological meaning. Nevertheless, this diagram shows some interesting and potentially useful relationships. It illustrates that the initial stage of albitization seen in the microcline–albite granite zone has actually increased the Rb/Sr ratios relative to the original granite. This can be explained either because Sr was lost during albitization of the plagioclase or because the microcline–albite granite samples had undergone a greater degree of magmatic plagioclase fractionation prior to albitization, whereas Rb was retained in the microcline. The second stage of complete albitization, on the other hand, shows Rb/Sr ratios close to zero, because of the extreme Rb loss during albitization of the microcline. This has effectively frozen the $^{87}Sr/^{86}Sr$ ratios at the time of albitization, thus yielding apparent 'initial' $^{87}Sr/^{86}Sr$ ratios of 0·725–0·735 (taken from the samples with the lowest Rb/Sr ratios). These are much higher than actual initial ratios of common A-type granites, which typically have initial $^{87}Sr/^{86}Sr$ ratios of about 0·705 (e.g. Anderson, 1983; Vander Auwera *et al.*, 2003). There are two possible interpretations of these high 'initial' ratios. (1) They might reflect radiogenic Sr in the infiltrating fluid, which derived its highly radiogenic Sr from the local country rocks depending on their age and composition. In this case the apparent isochron would be a mixing line generated by Sr from the granite and radiogenic Sr from the fluid, and neither the 'isochron' nor the 'initial ratio' would reflect any particular age. One argument in favour of this interpretation is the obviously open-system behaviour of Rb (and possibly also Sr) in these rocks. (2) If Sr was not added in significant amounts, and Rb was removed more effectively during albitization, then the 'frozen' $^{87}Sr/^{86}Sr$ ratio would reflect radiogenic ingrowth between the time of granite emplacement and the time of Rb removal. In this case, a simple model calculation, assuming that the initial $^{87}Sr/^{86}Sr$ of the granite was ∼0·705 and the average $^{87}Rb/^{86}Sr$ of the initial granites was ∼7·9, yields a time difference between emplacement and albitization of about 300 Myr. This estimate suffers from the considerable uncertainty in the mean actual Rb/Sr ratio of the granite, because all of the samples studied have undergone variable degrees of feldspar fractionation prior to final emplacement (Kaur *et al.*, 2006), and this would have severely affected the Rb/Sr ratio. Nevertheless, this estimate is consistent (within error) with the apparent Sm–Nd isochron age of about 1460 Ma of the albite granite. This time interval (300 Myr) would be sufficient to cool the granite intrusions to the ambient temperature of the country rocks. For this reason, we investigate internal heat production of the granite as a possible alternative heat source driving the metasomatic process (see below).

Although the whole-rock $\delta^{18}O$ values fall within the range of '^{18}O-normal' granitoid rocks ($\delta^{18}O = +6$ to $+10‰$; Taylor, 1978), they steadily increase with progressive albitization and silicification (Fig. 9). It should be noted for the Dosi granites that during the transformation of the original granite to the microcline–albite granite, there is only a minor increase in both whole-rock and mineral phase $\delta^{18}O$ (Table 4), which may be attributed to the crystallization of new, isotopically heavy, quartz and the replacement of oligoclase by heavy albite. In contrast, there is substantial increase in $\delta^{18}O$ values for both whole-rock and mineral phases during the transformation of the microcline–albite granite to the albite granite, which may be partly linked to the replacement of microcline by heavy albite, together with the crystallization of isotopically heavier Si-rich phases (actinolite and albite) and recrystallization of already existing quartz to larger strain-free heavy crystals. Therefore, part of the whole-rock $\delta^{18}O$ increase is probably related to these mineralogical changes. The feldspars in the microcline–albite granite are brick red in colour, which may be due to the presence of hematite inclusions, which can be observed using a binocular microscope, and indicate precipitation of ferric iron oxides from a fluid within the feldspar pores (Putnis *et al.*, 2007; Plümper & Putnis, 2009). Such reddening of feldspars is usually accompanied by reversed or negative ΔQtz–Fsp isotopic fractionation (e.g. Taylor, 1978) implying that in such cases, quartz–feldspar pairs are strongly out of isotopic equilibrium (Wenner & Taylor, 1976). However, this

is not the case in the present study, as ΔQtz–Fsp values show a normal or positive (around +1 to + 2‰) fractionation trend, indicating an alteration temperature that was sufficient to re-equilibrate the magmatic assemblage with the hydrothermal fluids. The systematic increase in the $\delta^{18}O$ values of quartz, feldspars and mafic phases from the moderately to the completely albitized granites further suggests that the temperature of the albitizing fluid was low at the time of alteration.

As demonstrated above, the albitizing fluid must have metasomatized the granites at temperatures well below any magmatic stage. The nature of this fluid could, in principle, be meteoric ground water or any surface-derived water (seawater or fresh water) or metamorphic water that had been modified through circulation in the crust. Meteoric or surface-derived waters are very low in $\delta^{18}O$ (e.g. in meteoric water, $\delta^{18}O$ is ~0 to −10‰; Sheppard, 1986) and would thus cause depletion in whole-rock $\delta^{18}O$ values by at least 6–12‰ (e.g. Taylor & Forester, 1971) rather than causing the enrichment observed. Therefore, a metamorphic fluid ($\delta^{18}O = +3$ to +20‰; Sheppard, 1986) that equilibrated with crustal rocks at metamorphic temperatures is the more likely candidate for supplying the high-$\delta^{18}O$ fluids that are suggested by our results.

Temperature of albitization

To estimate the temperature of albitization, we have followed initially the approach of Lee & Parsons (1997) using two-feldspar geothermometry. In practice, feldspar geothermometers yield the temperatures at which the coexisting feldspars achieved equilibrium, although it is not always straightforward to establish equilibrium in pairs of feldspars. In particular, when a mineral is replaced by a metasomatic front, local equilibrium is expected to exist within each zone, but minerals separated by a replacement front are not expected to be in equilibrium (see below). Nevertheless, the coexistence of pure albite with orthoclase-rich, albite-poor K-feldspar and their nearly constant composition (i.e. a total lack of zonation) suggest that, within a single sample and during the various stages of albitization, at least local equilibrium was attained between these two feldspars. This conforms to the fact that, at complete equilibrium, a rock can contain not more than two feldspar phases at any temperature (Lee & Parsons, 1997). Therefore, temperatures of coexisting feldspar pairs were calculated using the program SOLVCALC (Wen & Nekvasil, 1994) and the thermometer of Fuhrman & Lindsley (1988). A pressure of 200 MPa was assumed for the emplacement of the studied granites (see Kaur *et al.*, 2006). Three temperatures, T_{Or}, T_{Ab} and T_{An}, were calculated based on the activity of each component (orthoclase, albite and anorthite) between K-feldspar and pure albite (Fuhrman & Lindsley, 1988). T_{dis} represents the equilibrium temperature for disordered feldspars deduced from T_{Or}, T_{Ab} and T_{An}, which was increased by about 100°C to account for the approximation of the equilibrium temperature (T_{ord}) for ordered feldspar pairs (Brown & Parsons, 1989). To test this assumption, an albite crystal of roughly one cubic millimeter in size was taken from sample DS-4 for characterization by powder X-ray diffraction. The lattice constants determined were

$$a = 8{\cdot}1514 \pm 0{\cdot}0003\text{Å}$$
$$b = 12{\cdot}8055 \pm 0{\cdot}0005\text{Å}$$
$$c = 7{\cdot}1648 \pm 0{\cdot}0003\text{Å}$$
$$\alpha = 94{\cdot}230 \pm 0{\cdot}003^\circ$$
$$\beta = 116{\cdot}599 \pm 0{\cdot}002^\circ$$
$$\gamma = 87{\cdot}788 \pm 0{\cdot}002^\circ$$

which conform to nearly pure, completely ordered low albite (e.g. Smith & Brown, 1988).

As the albitization of both K-feldspar and plagioclase has produced pure albite of similar composition, a number of feldspar pairs (pure albite and microcline) have been used to constrain equilibration temperatures; their average values are shown in Table 5. The temperatures obtained for the three feldspar components between two coexisting feldspars in all the samples are concordant, which further supports the assumption that the feldspar compositions represent equilibrium (Fuhrman & Lindsley, 1988).

The temperature estimates from the two-feldspar thermometer in the albitized granites yield a disordered temperature (T_{dis}) range of 255–294°C, corresponding to an ordered temperature (T_{ord}) range of 355–395°C. The accuracy of such low temperatures may be poor (see Lee & Parsons, 1997), but the excellent concordance in the temperatures of all the three components of feldspars indicate that our temperature estimates are likely to be reasonably accurate.

As explained above, albitization took place at temperatures high enough to allow the re-equilibration of the magmatic assemblage. We can therefore use the quartz–feldspar oxygen isotope fractionation as an additional estimate of the temperature of albitization. We have calculated apparent temperatures from the $\delta^{18}O$ data for quartz and feldspars for all the moderately and completely albitized granites, using the ΔQtz–Ab calibration of Clayton & Kieffer (1991) and Zheng (1993). The analytical uncertainty for each mineral analysis is 0·16‰, corresponding to a total error of 0·23‰ for the ΔQtz–Ab fractionation. This translates into a temperature uncertainty of around ±50°C for the quartz–albite pairs in the completely albitized samples. In the case of the moderately albitized granites, which contain albite as well as K-feldspar, the temperature uncertainty is up to 40°C higher because the calculated quartz–albite temperatures neglect any

Table 5: Temperature (°C) estimates from the two-feldspar geothermometer (Fuhrman & Lindsley, 1988) for the A-type albitized granites, Rajasthan, NW India

Sample	Rock type	Plagioclase			K-feldspar			T_{Ab}	T_{Or}	T_{An}	n	T_{Dis}	T_{Ord}
		Ab	Or	An	Ab	Or	An						
Biharipur pluton													
BH-17	Mc–Ab granite	98·8	0·7	0·5	4·9	95·1	0·0	262	262	262	7	262 ± 12	365
BH-24	Mc–Ab granite	96·4	1·3	2·3	5·0	95·0	0·0	270	270	270	8	270 ± 17	370
BH-58	Mc–Ab granite	98·5	0·7	0·8	4·8	95·2	0·0	260	260	260	7	260 ± 9	360
BH-8	Ab granite	98·2	1·0	0·8	4·9	95·1	0·0	275	275	275	6	275 ± 14	375
Dabla pluton													
DB-9	Mc–Ab granite	98·8	0·5	0·7	4·8	95·2	0·0	261	261	261	6	261 ± 17	365
DB-11	Mc–Ab granite	98·5	0·6	0·9	5·2	94·8	0·0	258	258	258	9	258 ± 7	360
DB-33	Mc–Ab granite	98·6	0·6	0·8	4·6	95·4	0·0	277	277	277	5	277 ± 15	380
DB-7	Trans. granite	98·8	0·5	0·7	4·6	95·4	0·0	255	255	255	6	255 ± 8	355
Dosi pluton													
DS-4	Mc–Ab granite	97·6	0·7	1·7	5·9	94·1	0·0	281	281	281	9	281 ± 14	385
DS-13	Trans. granite	97·9	0·8	1·3	6·4	93·6	0·0	294	294	294	4	294 ± 16	395

n, number of feldspar pairs used to calculate the temperatures; T_{Dis}, equilibrium temperature for disordered feldspars; T_{Ord}, approximate equivalent temperatures for ordered feldspars, which is ~100°C more than the T_{Dis} (Brown & Parsons, 1989). Mc, microcline; Ab, albite; Trans., Transitional.

fractionation that may occur between albite and K-feldspar, which in any case is considered to be very small (<0·2‰ at 400°C, e.g. Bottinga & Javoy, 1973; Zheng, 1993).

Using the calibration of Zheng (1993), the quartz–feldspar pairs in which ΔQtz–Ab/Fsp fractionation is around 2‰ yield temperatures in the range of 345–392°C (Table 4), whereas those of Clayton & Keiffer (1991) give about 30–40°C higher temperature estimates. These temperature estimates, within error, are similar to those determined from the feldspar thermometry. We thus conclude that albitization of the Khetri granites took place at ~350–400°C. Similar temperatures for albitization have been estimated from other regions; for example, 250–400°C for the Bohus granite, Sweden (Petersson & Eliasson, 1997), ~370°C for the Shap granite, England (Lee & Parsons, 1997), 350–450°C for an albitized granitic pegmatite of the Bamble sector, Norway (Nijland & Touret, 2001) and ~400°C for the peraluminous albitized granites of Salvezines Massif, French Pyrénées (Boulvais *et al.*, 2007).

Some samples, most notably DB-33 (Table 4), where the ΔQtz–Ab/Fsp fractionation factors are either less or more than 2‰, yield unlikely temperature estimates. There may be several reasons for this 'misbehaviour'. For example, oxygen diffusion is relatively fast in quartz and feldspars (e.g. Brady, 1995), suggesting that quartz–feldspar temperatures in granites can record stages well below the solidus. Given that the closure of a system is strongly dependent on the grain size (e.g. Dodson, 1973), it is conceivable that some of the recorded variations in ΔQtz–Ab/Fsp may be due to closure of isotopic exchange at slightly different temperatures in different samples. These arguments, along with the analytical error, could explain the moderate deviations of ΔQtz–Ab/Fsp in samples DB-37 and DS-4 (Table 4). Nevertheless, the lowest value of ΔQtz–Ab/Fsp in sample DB-33 is difficult to explain by these mechanisms, suggesting that this sample failed to equilibrate.

Metasomatic infiltration model

The following conceptual, and slightly idealized metasomatic model for the albitization observed in the Khetri granites corresponds closely to the mechanism of pure infiltration metasomatism proposed by Korzhinskii (1968) and applied to alkali feldspars (Hofmann, 1972), as follows.

(1) After intrusion and crystallization of the granitoid magma, the single plutons cooled to essentially ambient temperatures of roughly 300–400°C at upper crustal levels. Such a scenario might normally lack the thermal gradients that drive extensive hydrothermal alteration in cooling igneous bodies.

However, these A-type granites have high internal heat production (Table 2) about four times that of average upper continental crust (Rudnick & Gao, 2003). Depending on the size of the granitoid body, this means that the long-term, steady-state temperature in the interior of these granites may be 30–100°C higher than that in the surrounding normal crust, provided that the (subsurface) dimensions of the granite bodies are substantially larger (10–20 km diameter) than the outcrop areas (2–3 km) of the plutons (see thermal modelling in the Appendix). The existence and compositional similarities of many small hillocks of granitoid protruding from the surrounding alluvium, as well as granitoid rocks recovered from surrounding wells, attest to the plausibility of this inference. If this is correct, then there will be long-term horizontal temperature gradients in the upper crust, which serve as potential heat pumps driving hydrothermal circulation. This circulation may have been activated on a regional scale during formation of the Khetri lineament.

(2) Hydrothermal circulation generally causes meteoric or metamorphic waters, which enter the crust in cool regions, to rise through hotter regions. In the present context, the high 'water–rock ratios' needed to albitize large volumes of granite ultimately point to a meteoric origin for the fluid, which has lost its oxygen isotope memory by exchanging oxygen with a large body of low-temperature metamorphic rocks. These waters will acquire high Na/K and Na/Ca ratios through low-temperature reaction with alkali feldspar in metasedimentary country rocks metamorphosed under greenschist-facies conditions (Orville, 1963; Moody *et al.*, 1985). When such a fluid enters a region with elevated temperatures, its Na/K ratio will be too high for it to coexist with K-feldspar. This is a consequence of the temperature dependence of the alkali feldspar–fluid equilibrium (Orville, 1963). Consequently, when a fluid with an Na/K ratio fixed by a large, external reservoir (i.e. the country rock) invades a two-feldspar granitoid, it will convert the two-feldspar assemblage into pure albite, provided that the temperature of the granitoid body is higher than that of the country rock, even if such a temperature difference is small.

A similar relationship is likely to hold for the Na/Ca ratio of the plagioclase peristerite gap, although the compositions of fluids in equilibrium with peristerites have, to our knowledge, not been determined experimentally. The net result of these phase relations is that a fluid (possibly in the form of an alkali chloride solution) equilibrated with a two-feldspar peristerite assemblage at low temperatures will produce a single albite phase if the temperature of the infiltrated rock body is higher than that of the surrounding source of the fluid.

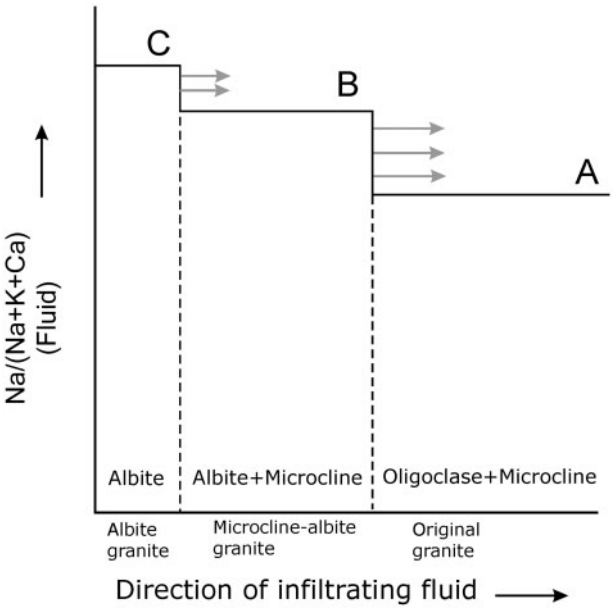

Fig. 12. Sketch representing the development of two sharp replacement fronts during albitization. The first, leading metasomatic front converts oligoclase to albite (B), and the second, trailing front replaces microcline with albite (C), leading to the formation of the microcline–albite granite and the albite granite, respectively. 'A' represents the original granite. The *x*-axis represents the distance from the point of fluid infiltration. The relative rates of migration of the two fronts are proportional to the ratio of the concentration differences of Na in the fluid and solid phases $\Delta C(\text{fluid})/\Delta C(\text{solid})$ across a given replacement front [see equation (6)].

(3) A simplified chromatographic infiltration model using the documented and inferred equilibria outlined above is shown in Fig. 12. Following the theoretical treatments of Korzhinskii (1968) and Hofmann (1972), the replacement fronts for plagioclase and K-feldspar advance at different rates as suggested by either the equation

$$\frac{\mathrm{d}z}{\mathrm{d}V} \propto \frac{\mathrm{d}C_\mathrm{f}}{\mathrm{d}C_\mathrm{s}} \tag{5}$$

or, in case of sharp fronts across solubility gaps (as well as certain continuous solid solutions; see Hofmann, 1972),

$$\frac{\mathrm{d}z}{\mathrm{d}V} \propto \frac{\Delta C_\mathrm{f}}{\Delta C_\mathrm{s}} \tag{6}$$

where $\mathrm{d}z/\mathrm{d}V$ is the rate of advance of the replacement front relative to the rate of advance of the carrier fluid, and ΔC_f and ΔC_s represent the concentration differences across the replacement front of the component in question (in this case Na) in the fluid and solid respectively. In other words, the rate of advance of the front replacing

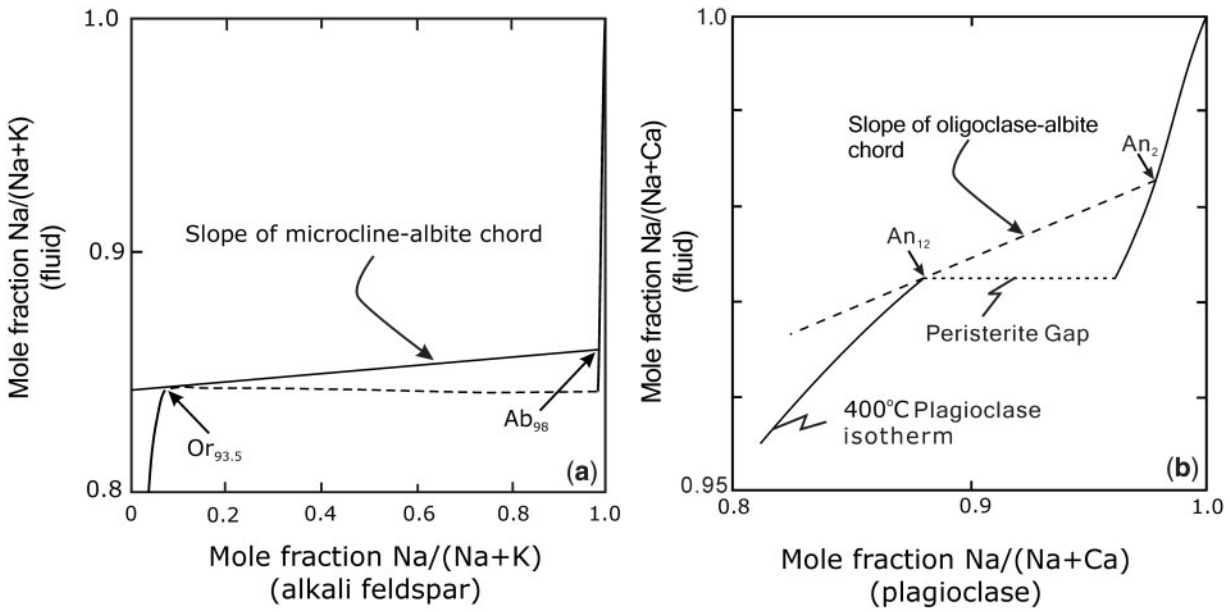

Fig. 13. (a) Estimated fluid–alkali feldspar distribution at 400°C and 200 MPa pressure for 2M aqueous chloride solutions (after Orville, 1963). The rate of advance of the infiltration front where albite replaces microcline (Fig. 12) is proportional to the slope of the chord connecting the composition of the final albite (Ab_{98}) with that of the microcline being replaced ($Or_{93·5}Ab_{6·5}$), as observed in Dosi granite feldspars [see equation (6); Table S1]. The slope of the chord connecting the microcline with the final albite composition is lower than that of the oligoclase–albite chord in (b) because of the large width of the solubility gap. In terms of the chromatographic model used here, this means that the microcline–albite front advances through the granites relatively slowly. (b) Estimated equilibrium distribution of Na/(Na + Ca) between fluid and K-free plagioclase at 400°C. The dashed line is the chord connecting the composition of the initial oligoclase with the final albite. Because of the narrow size of the peristerite solubility gap, this slope is relatively steep, even for the relatively small increase of Na/(Na + Ca) in the fluid compositions. Therefore, the metasomatic front replacing oligoclase by albite migrates more rapidly than the trailing front replacing microcline by albite.

oligoclase or microcline by albite is proportional to the slope of the line, $\Delta C_f/\Delta C_s$, connecting the final composition with the initial composition as shown in Fig. 13a and 13b, respectively.

A difficulty in the present case is that ternary equilibrium data for the Ca–K–Na concentrations of fluids in equilibrium with the feldspars are not available. However, the two replacement fronts displayed by our granites represent nearly binary reactions, so the existing experimental data for binary feldspar systems can be used as guidelines. The plagioclase equilibria have been determined only at 700°C (Orville, 1972; Shmulovich & Graham, 2008), a temperature much higher than is applicable to our setting where plagioclase compositions are 'interrupted' by the peristerite gap. Nevertheless, the high-temperature data allow us to estimate an approximate phase equilibrium at temperatures low enough for the peristerite solubility gap to exist. Figure 13b shows such a hypothetical equilibrium that is qualitatively similar to the higher temperature equilibrium of Orville (1972), except that the continuous solid plagioclase solution is replaced by a peristerite gap. Orville also emphasized that the Na/Ca ratio of the fluid coexisting with a given plagioclase will shift to lower values as pressure decreases (whereas the effect of temperature is relatively small). This means that an ascending fluid (with its Na/Ca ratio imposed at higher pressure conditions) will convert all the oligoclase to albite.

The experimental basis for the alkali feldspar system (Fig. 13a) is much more firmly established. Orville (1963) estimated a minimum ratio of Na/(K + Na) ≥ 0·84 for a 2M NaCl solution at 200 MPa and 400°C. As explained above, a fluid that had its Na/K ratio fixed in an external, low-temperature environment will convert all K-feldspar to albite when it infiltrates into a higher-temperature granitoid, with only a minor pressure effect.

The actual changes in fluid composition (Na/Ca and Na/K) are not known in detail, but may well be fairly small in both cases. The change in solid composition is, however, obviously much higher in case of the microcline–albite conversion than for oligoclase to albite. Consequently, the slope of the chord connecting the microcline to albite will be significantly lower than the slope of the oligoclase–albite chord. Therefore, following equation (6), the microcline–albite front will lag behind the oligoclase–albite front. Thus, a single infiltration event into a permeable rock matrix can form a leading replacement front where plagioclase is converted into albite, and a trailing, slower-moving front where K-feldspar is replaced by

albite. Such sharp replacement fronts between microcline–albite granites and albite granites are well displayed in several outcrops in the study area, where they are marked by prominent colour differences (Fig. 3b).

The model specifically explains the observed discrete nature of the metasomatized rock types encountered. Metasomatic infiltration, under conditions of local equilibrium, will always produce sharp replacement fronts whenever the minerals involved have solubility gaps. There are, however, several details that are not specifically accounted for by the model. Among them are the concomitant changes and ultimate disappearance of the ferromagnesian minerals, as well as the addition of quartz. A more complete treatment of all these metasomatic changes may be possible using numerical simulations in conjunction with a thermodynamic database (see, e.g. Heinrich *et al.*, 1996), but such simulations are beyond the scope of this study. The first-order phenomena (two successive feldspar replacement fronts) can be well understood using the simpler Korzhinskii-type theory. Another question that may be more fully answered by future investigations is whether the high U–Th–K contents of A-type granites, and the resulting high heat production of such bodies, can be generalized to provide a widely applicable process for driving both albitization and metallogenic mineralization.

REGIONAL ASPECTS OF ALBITIZATION

Ray (1990) postulated a 170 km long NNE–SSW-trending lineament in the NW Indian shield and called it the 'albitite line' because numerous albitites occur all along this lineament with associated fluorite–ilmenite–magnetite–uraninite–sulphide mineralization. Envisaging a purely magmatic origin for these rocks, Ray (1990) considered this magmatism to be intraplate and anorogenic. Subsequent work, however, has made clear that these albitites are the products of Na-metasomatism (e.g. Sinha *et al.*, 2000). Yadav *et al.* (2000) termed the albitite line a 'zone of alkali metasomatism' and also broadened this zone by shifting its eastern and western limits, so that it now includes some of the granitoid plutons of the Khetri complex. The albitized alkali-feldspar granites of Biharipur and Dabla fall within this zone of alkali metasomatism, which we have extended farther to the NE to include the similar granites of Dosi (Fig. 1a). The Atomic Minerals Division of India has discovered several uranium occurrences associated with the albitized rocks of this region (e.g. Jain *et al.*, 1999; Yadav *et al.*, 2000). Sharma *et al.* (2000) reported U–Th–Y mineralization in albitized dykes of alkali-feldspar granite within the granitoids of the Dhanota pluton, which is an intervening intrusive body between the Dosi and Biharipur–Dabla plutons (Fig. 1a). In the southern Khetri complex, uranium mineralization, which occurs mainly as veins and fracture fillings, is essentially controlled by and confined to weak planes in albitized metasediments and igneous intrusive rocks (e.g. Pradeep Kumar *et al.*, 2009). There thus seems to be a genetic relationship between albitization and uranium mobilization in the region.

Our preliminary studies (Kaur *et al.*, 2011*a*) also document the presence of moderately and completely albitized granites in some of the granitoid plutons of the southern Khetri complex (e.g. Mandaora and Gowariyan). Moreover, the Alwar region, which is located about 95 km SE of Khetri, also includes albitized granites (e.g. Harsora and Ajitgarh) of similar age to those of Khetri (P. Kaur *et al.*, unpublished data). Therefore, it is evident that albitization is not a local phenomenon, but is widespread in the northern part of the Aravalli mountain range. The Khetri region experienced A-type, within-plate, felsic magmatic activity at around 1700 Ma (Kaur *et al.*, 2007, 2011*a*). Nearly all of these granitoids are albitized, and are aligned along the NE–SW-trending Khetri lineament. The pervasive nature of the albitization suggests that the reactivation of the Khetri lineament (see Yadav *et al.*, 2000), as well as the deformed nature of the granites, probably provided conduits for the migration of large volumes of albitizing fluids. This is also indicated by the extensive IOCG mineralization in the Khetri complex. The driving force for moving these fluids on a large scale may have been provided by the thermal gradients generated by the widespread occurrence of high heat production, A-type granites in this region. Much more detailed geochronological work, however, will be needed to establish the temporal relations between the granite intrusion, the albitization and the general mineralization in the Khetri complex.

CONCLUSIONS

(1) Infiltration of low-temperature, Na-rich fluid has albitized the original granite in two discrete steps. A leading metasomatic front converted the original oligoclase into albite with crystallization of new quartz to form the pink microcline–albite granite. This was followed by a more slowly moving second replacement front, which eliminated the K-feldspar and converted the microcline–albite granite into a pure, generally white, albite granite along with formation of new Si-rich phases and recrystallization of new quartz.

(2) The contacts between the albite granite and microcline–albite granite are sharp, consistent with the theory of infiltration metasomatism.

(3) The initial increase followed by a sudden drop in the X_{Fe} values of amphiboles correlates with the

transformation of potassian ferropargasite in the original granite to potassic hastingsite and finally to actinolite–magnesiohornblende in the albitized granites.

(4) During albitization there is significant hydration, minor gain of Si and loss of Ca (and Fe, Mg, Rb, Sr, P, Ti, etc.) in the first stage of metasomatism, whereas the second and final stage caused a major gain in Na (without any further hydration), and substantial loss of K, Rb and Ba, accompanied by less extreme, but still large, losses of Fe, Mg, Ca, Sr, Zn, La and all but the heaviest other REE.

(5) Sm–Nd and Rb–Sr isotope systematics demonstrate open-system behaviour during albitization. A poorly defined Sm–Nd errorchron of about 1460 Ma and the highly radiogenic $^{87}Sr/^{86}Sr$ ratios at very low Rb/Sr ratios of the albite granites both point to a minimum time lag of roughly 300 Myr between magmatic emplacement and albitization.

(6) Albitization occurred at temperatures of ~350–400°C, and was induced by meteoric waters that attained high-$\delta^{18}O$ isotope compositions by exchanging oxygen with metamorphic fluids.

(7) Regional considerations show that the northern Aravalli mountain range records a widespread event of sodium metasomatism; the dominance of albitization appears to be tectonically controlled.

(8) The widespread occurrence of high heat production, A-type granite bodies may have provided the heat source for driving the albitizing fluids.

ACKNOWLEDGEMENTS

We acknowledge Rosemarie Baur (Würzburg) for carefully performing XRF analyses, Uli Schüssler (Würzburg), Dmitry V. Kuzmin and Nora Groschopf (both Mainz) for their assistance during the microprobe work, Doris Neuhäuser (Mainz) for help in the clean laboratory, and Reinhard Neder (Würzburg) for providing X-ray diffraction data. We are grateful to Philippe Boulvais, Ane Engvik and Gregor Markl for providing extremely thorough and constructive comments on an earlier version of the paper. The subsequent versions were considerably improved by in-depth and insightful reviews by James A. Grant, Patrizia Fiannacca, Marlina Elburg, Daniel Harlov, Mark Barton and Roberto Dall'Agnol, and the editorial handling of Reto Gieré. This is a contribution to the IGCP-510 project: A-type granites and related rocks through time.

FUNDING

Financial assistance to P. Kaur from the German Academic Exchange Service (DAAD), Bonn (No. A/03/02882) is gratefully acknowledged.

SUPPLEMENTARY DATA

Supplementary data for this paper are available at *Journal of Petrology* online.

REFERENCES

Anderson, G. H. (1937). Granitization, albitization, and related phenomena in the northern Inyo range of California–Nevada. *Geological Society of America Bulletin* **48**, 1–74.

Anderson, J. L. (1983). Proterozoic anorogenic granite plutonism of North America. In: Medaris, L. G. Jr., Byers, C. W., Mickelson, D. M. & Shanks, W. C. (eds) *Proterozoic Geology. Geological Society of America, Memoirs* **161**, 133–154.

Baker, J. H. (1985). Rare earth and other trace element mobility accompanying albitization in a Proterozoic granite, W. Bergslagen, Sweden. *Mineralogical Magazine* **49**, 107–115.

Barker, F. (1979). Trondhjemite: definition, environment and hypothesis of origin. In: Barker, F. (ed.) *Trondhjemites, Dacites and Related Rocks*. Amsterdam: Elsevier, pp. 1–12.

Barton, M. D. & Johnson, D. A. (1996). Evaporitic-source model for igneous-related Fe-oxide–(REE–Cu–Au–U) mineralization. *Geology* **24**, 259–262.

Basu, S. K. & Narsayya, B. L. (1983). A probable zone of carbonatite and fenitic rock association in the eastern part of the Khetri Copper Belt, northeastern Rajasthan. *Geological Survey of India Records* **113**, 7–15.

Bea, F. (1996). Residence of REE, Y, Th and U in granites and crustal protoliths; implications for the chemistry of crustal melts. *Journal of Petrology* **37**, 521–552.

Beardsmore, G. R. & Cull, J. P. (2001). *Crustal Heat Flow: A Guide to Measurement and Modelling*. Cambridge: Cambridge University Press, 324 p.

Biju-Sekhar, S., Yokoyama, K., Pandit, M. K., Okudaira, T., Yoshida, M. & Santosh, M. (2003). Late Paleoproterozoic magmatism in Delhi Fold Belt, NW India and its implication: evidence from EPMA chemical ages of zircons. *Journal of Asian Earth Sciences* **22**, 189–207.

Bottinga, Y. & Javoy, M. (1973). Comments on oxygen isotope geothermometry. *Earth and Planetary Science Letters* **20**, 250–265.

Boulvais, P., Ruffet, G., Cornichet, J. & Mermet, M. (2007). Cretaceous albitization and dequartzification of Hercynian peraluminous granite in the Salvezines Massif (French Pyrénées). *Lithos* **93**, 89–106.

Brady, J. B. (1995). Diffusion data for silicate minerals, glasses, and liquids. In: Ahrens, T. J. (ed.) *Mineral Physics and Crystallography: A Handbook of Physical Constants. American Geophysical Reference Shelf* **2**, 269–290.

Brown, W. L. & Parsons, I. (1989). Alkali feldspars: ordering rates, phase transformations and behaviour diagrams for igneous rocks. *Mineralogical Magazine* **53**, 25–42.

Carslaw, H. S. & Jaeger, J. C. (1959). *Conduction of Heat in Solids*, 2nd edn. Oxford: Clarendon Press, 510 p.

Carten, R. B. (1986). Sodium–calcium metasomatism: chemical, temporal, and spatial relationships at the Yerington, Nevada, porphyry copper deposit. *Economic Geology* **81**, 1495–1519.

Cathelineau, M. (1986). The hydrothermal alkali metasomatism effects on granitic rocks: quartz dissolution and related subsolidus changes. *Journal of Petrology* **27**, 945–965.

Charoy, B. & Pollard, P. J. (1989). Albite-rich, silica-depleted metasomatic rocks at Emuford, northeast Queensland: mineralogical,

geochemical, fluid inclusion constraints on hydrothermal evolution and tin mineralization. *Economic Geology* **84**, 1850–1874.

Chaudhri, N., Kaur, P., Okrusch, M. & Schimrosczyk, A. (2003). Characterisation of the Dabla granitoids, North Khetri Copper Belt, Rajasthan, India: evidence of bimodal anorogenic felsic magmatism. *Gondwana Research* **6**, 879–895.

Clayton, R. N. & Kieffer, S. W. (1991). Oxygen isotopic thermometer calibrations. In: Taylor, H. P., O'Neil, J. R. & Kaplan, I. R. (eds) *Stable Isotope Geochemistry: A Tribute to Samuel Epstein. Geochemical Society, Special Publication* **3**, 3–10.

Costi, H. T., Dall'Agnol, R., Borges, R. M. K., Minuzzi, O. R. R. & Teixeira, J. T. (2002). Tin-bearing sodic episyenites associated with the Proterozoic, A-type Água Boa granite, Pitinga Mine, Amazonian Craton, Brazil. *Gondwana Research* **5**, 435–451.

Dall'Agnol, R., Scaillet, B. & Pichavant, M. (1999). An experimental study of a Lower Proterozoic A-type granite from the eastern Amazonian Craton, Brazil. *Journal of Petrology* **40**, 1673–1698.

Das Gupta, S. P. (1968). *The Structural History of the Khetri Copper Belt, Jhunjhunu and Sikar Districts, Rajasthan. Geological Survey of India Memoirs* **98**, 170 p.

Dey, R. C. (1985). Polyphase folding deformation in the Delhi Supergroup of rocks in southern Haryana, India. *Indian Minerals* **39**, 42–60.

Dodson, M. (1973). Closure temperature in cooling geochronological and petrological systems. *Contributions to Mineralogy and Petrology* **40**, 259–274.

Drummond, M. S., Ragland, P. C. & Wesolowski, D. (1986). An example of trondhjemite genesis by means of alkali metasomatism: Rockford Granite, Alabama Appalachians. *Contributions to Mineralogy and Petrology* **93**, 98–113.

Eby, G. N. (1990). The A-type granitoids: a review of their occurrence and chemical characteristics and speculations on their petrogenesis. *Lithos* **26**, 115–134.

Elburg, M. A., Bons, P. D., Dougherty-Page, J., Janka, C. E., Neumann, N. & Schaefer, B. (2001). Age and metasomatic alteration of the Mt Neil Granite at Nooldoonooldoona Waterhole, Mt Painter Inlier, South Australia. *Australian Journal of Earth Sciences* **48**, 721–730.

Engvik, A. K., Putnis, A., Fitz Gerald, J. D. & Austrheim, H. (2008). Albitization of granitic rocks: the mechanism of replacement of oligoclase by albite. *Canadian Mineralogist* **46**, 1401–1415.

Fiannacca, P., Brotzu, P., Cirrincione, R., Mazzoleni, P. & Pezzino, A. (2005). Alkali metasomatism as a process for trondhjemite genesis: evidence from Aspromonte Unit, north-eastern Peloritani, Sicily. *Mineralogy and Petrology* **84**, 19–45.

Frost, B. R. & Frost, C. D. (2008). A geochemical classification for feldspathic igneous rocks. *Journal of Petrology* **49**, 1955–1969.

Frost, B. R., Barnes, C. G., Collins, W. J., Arculus, R. J., Ellis, D. J. & Frost, C. D. (2001). A geochemical classification for granitic rocks. *Journal of Petrology* **42**, 2033–2048.

Fuhrman, M. L. & Lindsley, D. H. (1988). Ternary-feldspar modeling and thermometry. *American Mineralogist* **73**, 201–215.

Geological Survey of India. (1997). *Geological Map of the North Khetri Copper Belt, Sikar and Jhunjhunu Districts, Rajasthan*. Jaipur: Geological Survey of India, scale 1:50 000.

Grant, J. A. (1986). The isocon diagram—a simple solution to Gresens' equation for metasomatic alteration. *Economic Geology* **81**, 1976–1982.

Grant, J. A. (2005). Isocon analysis: a brief review of the method and applications. *Physics and Chemistry of the Earth* **30**, 997–1004.

Gupta, S. N., Arora, Y. K., Mathur, R. K., Iqbaluddin, Prasad, B., Sahai, T. N. & Sharma, S. B. (1997). *The Precambrian Geology of the Aravalli Region, Southern Rajasthan and Northeastern Gujarat. Geological Survey of India Memoirs* **123**, 262 p.

Heinrich, C. A., Walshe, J. L. & Harrold, B. P. (1996). Chemical transfer modeling of ore-forming hydrothermal systems: current practice and problems. *Ore Geology Reviews* **10**, 319–338.

Hermann, J. (2002). Allanite: thorium and light rare earth element carrier in subducted crust. *Chemical Geology* **192**, 289–306.

Heron, A. M. (1923). Geology of western Jaipur. *Geological Survey of India Records* **54**, 345–397.

Hofmann, A. (1972). Chromatographic theory of infiltration metasomatism and its application to feldspar. *American Journal of Science* **272**, 69–90.

Hövelmann, J., Putnis, A., Geisler, T., Schmidt, B. C. & Golla-Schindler, U. (2010). The replacement of plagioclase feldspars by albite: observations from hydrothermal experiments. *Contributions to Mineralogy and Petrology* **159**, 43–59.

Jacobsen, S.T. B. & Wasserburg, G. J. (1980). Sm–Nd isotopic evolution of chondrites. *Earth and Planetary Science Letters* **50**, 139–155.

Jain, R. B., Yadav, O. P., Rahman, M., Thippeswamy, S., Fahmi, S., Sharma, D. K. & Singh, G. (1999). Petrography and geochemistry of the radioactive albitites and their genesis: Maonda area, Rajasthan. *Journal of the Geological Society of India* **53**, 407–415.

Kaur, P., Chaudhri, N., Okrusch, M. & Koepke, J. (2006). Palaeoproterozoic A-type felsic magmatism in the Khetri Copper Belt, Rajasthan, northwestern India: petrologic and tectonic implications. *Mineralogy and Petrology* **87**, 81–122.

Kaur, P., Chaudhri, N., Raczek, I., Kröner, A. & Hofmann, A. W. (2007). Geochemistry, zircon ages and whole-rock Nd isotopic systematics for Palaeoproterozoic A-type granitoids in the northern part of the Delhi belt, Rajasthan, NW India: implications for late Palaeoproterozoic crustal evolution of the Aravalli craton. *Geological Magazine* **144**, 361–378.

Kaur, P., Chaudhri, N., Raczek, I., Kröner, A. & Hofmann, A. W. (2009). Record of 1·82 Ga Andean-type continental arc magmatism in NE Rajasthan, India: insights from zircon and Sm–Nd ages, combined with Nd–Sr isotope geochemistry. *Gondwana Research* **16**, 56–71.

Kaur, P., Zeh, A., Chaudhri, N., Gerdes, A. & Okrusch, M. (2011*b*). Archaean to Palaeoproterozoic crustal evolution of the Aravalli mountain range, NW India, and its hinterland: the U–Pb and Hf isotope record of detrital zircon. *Precambrian Research* **187**, 155–164.

Kaur, P., Chaudhri, N., Raczek, I., Kröner, A., Hofmann, A. W. & Okrusch, M. (2011*a*). Zircon ages of late Palaeoproterozoic (*ca.* 1·72–1·70 Ga) extension-related granitoids in NE Rajasthan, India: regional and tectonic significance. *Gondwana Research* **19**, 1040–1053.

Knight, J., Lowe, J., Joy, S., Cameron, J., Merrillees, J., Nag, S., Shah, N., Dua, G. & Jhala, K. (2002). The Khetri Copper Belt, Rajasthan: iron oxide copper–gold terrane in the Proterozoic of NW India. In: Porter, T. M. (ed.) *Hydrothermal Iron Oxide Copper–Gold and Related Deposits: A Global Perspective, Vol. 2*. Adelaide: PGC Publishing, pp. 321–341.

Korzhinskii, D. S. (1968). The theory of metasomatic zoning. *Mineralium Deposita* **3**, 222–231.

Kretz, R. (1983). Symbols for rock-forming minerals. *American Mineralogist* **68**, 277–279.

Lal, R. K. & Shukla, R. S. (1975). Low-pressure regional metamorphism in the northern portion of the Khetri Copper Belt of Rajasthan, India. *Neues Jahrbuch für Mineralogie, Abhandlungen* **124**, 294–325.

Leake, B. E., Woolley, A. R., Arps, C. E. S., Birch, W. D., Gilbert, M. C., Grice, J. D., Hawthorne, F. C., Kato, A., Kisch, H. J., Krivovichev, V. G., Linthout, K., Laird, J. & Mandarino, J. (1997). Nomenclature of amphiboles: report of the subcommittee on

amphiboles of the International Mineralogical Association Commission on new minerals and mineral names. *Mineralogical Magazine* **61**, 295–321.

Leake, B. E., Woolley, A. R., Birch, W. D., Burke, E. A. J., Ferraris, G., Grice, J. D., Hawthorne, F. C., Kisch, H. J., Krivovichev, V. G., Schumacher, J. C., Stephenson, N. C. N. & Whittaker, E. J. W. (2004). Nomenclature of amphiboles: additions and revisions to the International Mineralogical Association's amphibole nomenclature. *European Journal of Mineralogy* **16**, 191–196.

Lee, M. R. & Parsons, I. (1997). Dislocation formation and albitization in alkali feldspars from the Shap granite. *American Mineralogist* **82**, 557–570.

Liew, T. C. & Hofmann, A. W. (1988). Precambrian crustal components, plutonic associations, plate environment of the Hercynian Fold Belt of central Europe: indications from a Nd and Sr isotopic study. *Contributions to Mineralogy and Petrology* **88**, 129–138.

Ludwig, K. R. (2003). *User's Manual for Isoplot 3.00: A Geochronological Toolkit for Microsoft Excel*. Berkeley Geochronology Centre, Special Publication **4**, 70 p.

Mahood, G. & Hildreth, W. (1983). Large partition coefficients for trace elements in high-silica rhyolites. *Geochimica et Cosmochimica Acta* **47**, 11–30.

Mark, G. (1998). Albitite formation by selective pervasive sodic alteration of tonalite plutons in the Cloncurry district, Queensland. *Australian Journal of Earth Sciences* **45**, 765–774.

McDonough, W. F. & Sun, S.-S. (1995). Composition of the Earth. *Chemical Geology* **120**, 223–253.

Moody, J. D., Jenkins, J. O. & Meyer, D. (1985). An experimental investigation of the albitization of plagioclase. *Canadian Mineralogist* **23**, 583–596.

Moore, D. E. & Liou, J. G. (1979). Chessboard-twinned albite from Franciscan metaconglomerates of the Diablo Range, California. *American Mineralogist* **64**, 329–336.

Mukhopadhyay, D., Bhattacharyya, T., Chattopadhyay, N., Lopez, R. & Tobisch, O. T. (2000). Anasagar gneiss: a folded granitoid pluton in the Proterozoic South Delhi Fold Belt, central Rajasthan. *Proceedings of the Indian Academy of Sciences (Earth and Planetary Sciences)* **109**, 21–37.

Niedermeier, D. R. D., Putnis, A., Geisler, T., Golla-Schindler, U. & Putnis, C. V. (2009). The mechanism of cation and oxygen isotope exchange in alkali feldspars under hydrothermal conditions. *Contributions to Mineralogy and Petrology* **157**, 65–76.

Nijland, T. G. & Touret, J. L. R. (2001). Replacement of graphic pegmatite by graphic albite–actinolite–clinopyroxene intergrowths (Mjåvatn, southern Norway). *European Journal of Mineralogy* **13**, 41–50.

Norberg, N., Neusser, G., Wirth, R. & Harlov, D. (2011). Microstructural evolution during experimental albitization of K-rich alkali feldspar. *Contributions to Mineralogy and Petrology* **162**, 531–546.

Orville, P. M. (1963). Alkali ion exchange between vapor and feldspar phases. *American Journal of Science* **261**, 201–237.

Orville, P. M. (1972). Plagioclase cation exchange equilibria with aqueous chloride solution: results at 700°C and 2000 bars in the presence of quartz. *American Journal of Science* **272**, 234–272.

Pant, N. C., Kundu, A. & Joshi, S. (2008). Age of metamorphism of Delhi Supergroup rocks—electron microprobe ages from Mahendragarh district, Haryana. *Journal of the Geological Society of India* **72**, 365–372.

Passchier, C. W. & Trouw, R. A. J. (2005). *Microtectonics*, 2nd edn. Berlin: Springer, 366 p.

Perez, R. J. & Boles, J. R. (2005). An empirically derived kinetic model for albitization of detrital plagioclase. *American Journal of Science* **305**, 312–343.

Petersson, J. & Eliasson, T. (1997). Mineral evolution and element mobility during episyenitization (dequartzification) and albitization in the postkinematic Bohus granite, southwest Sweden. *Lithos* **42**, 123–146.

Plümper, O. & Putnis, A. (2009). The complex hydrothermal history of granitic rocks: multiple feldspar replacement reactions under subsolidus conditions. *Journal of Petrology* **50**, 967–987.

Porto da Silveira, C. L., Schorscher, H. D. & Miekeley, N. (1991). The geochemistry of albitization and related uranium mineralization, Espinhares, Paraiba (PB), Brazil. *Journal of Geochemical Exploration* **40**, 329–347.

Pradeep Kumar, T. B., Tiwari, A. & Fahmi, S. (2009). Nature of uranium mineralisation in the Kerpura-Tiwari-ka-bas area, Sikar district, Rajasthan. *Journal of the Geological Society of India* **73**, 220–228.

Putnis, A. & Putnis, C. V. (2007). The mechanism of reequilibration of solids in the presence of a fluid phase. *Journal of the Solid State Chemistry* **180**, 1783–1786.

Putnis, A., Hinrichs, R., Putnis, C. V., Golla-Schindler, U. & Collins, L. G. (2007). Hematite in porous red-clouded feldspars: evidence of large-scale crustal fluid–rock interaction. *Lithos* **95**, 10–18.

Ray, S. K. (1990). The albitite line of northern Rajasthan—A fossil intracontinental rift zone. *Journal of the Geological Society of India* **36**, 413–423.

Rodriguez-Carvajal, J. (2001). Recent developments of the program FULLPROF. *Commission on Powder Diffraction (IUCr) Newsletter* **26**, 12–19.

Roy, A. B. (1988). Stratigraphic and tectonic framework of the Aravalli mountain range. In: Roy, A. B. (ed.) *Precambrian of the Aravalli Mountain, Rajasthan, India. Memoir of the Geological Society of India* **7**, 3–31.

Roy, A. B. & Jakhar, S. R. (2002). *Geology of Rajasthan (Northwest India) Precambrian to Recent*. Jodhpur: Scientific Publishers (India), 421 p.

Rudnick, R. L. & Gao, S. (2003). Composition of the continental crust. In: Holland, H. D. & Turekian, K. K. (eds) *Treatise on Geochemistry, Vol. 3, The Crust*. Amsterdam: Elsevier, pp. 1–64.

Sarkar, S. C. & Dasgupta, S. (1980). Geologic setting, genesis and transformation of the sulfide deposits in the northern part of the Khetri copper belt, Rajasthan, India—an outline. *Mineralium Deposita* **15**, 117–137.

Sharma, G. S., Purohit, R. K., Roy, M., Sengupta, B. & Singh, J. (2000). Geochemistry and petrography of U–Th–Y mineralisation in alkali feldspar granite (alaskite) dykes around Dhanota, Mahendragarh district, Haryana, India. *Journal of the Geological Society of India* **55**, 189–196.

Sharp, Z. D. (1992). *In situ* laser microprobe techniques for stable isotope analysis. *Chemical Geology* **101**, 3–19.

Sheppard, S. M. F. (1986). Characterization and isotopic variations in natural waters. In: Valley, J. W., Taylor, H. P. & O'Neil, J. R. (eds) *Stable Isotopes in High Temperature Geological Processes. Mineralogical Society of America, Reviews in Mineralogy* **16**, 165–184.

Shmulovich, K. I. & Graham, C. (2008). Plagioclase–aqueous solution equilibrium: concentration dependence. *Petrology* **16**, 177–192.

Sinha, D. K., Fahmi, S., Bhatt, A. K., Singh, G. & Singh, R. (2000). Evidences of soda metasomatism in Ladera–Sakhun area, northeastern Rajasthan. *Journal of the Geological Society of India* **56**, 573–582.

Sinha-Roy, S., Malhotra, G. & Mohanty, M. (1998). *Geology of Rajasthan*. Bangalore: Geological Society of India, 278 p.

Slaby, E. (1992). Changes in the structural state of secondary albite during progressive albitization. *Neues Jahrbuch für Mineralogie, Monatshefte* **1992**, 321–335.

Smith, J. V. (1974). *Feldspar Minerals, Vol. 2, Chemical and Textural Properties*. Berlin: Springer, 690 p.

Smith, J. V. & Brown, W. L. (1988). *Feldspar Minerals, Vol. 1, Crystal Structures, Physical, Chemical and Microtextural Properties*, 2nd edn. Berlin: Springer, 828 p.

Streckeisen, A. L. (1976). To each plutonic rock its proper name. *Earth-Science Reviews* **12**, 1–33.

Taylor, H. P. (1978). Oxygen and hydrogen isotope studies of plutonic granitic rocks. *Earth and Planetary Science Letters* **38**, 177–210.

Taylor, H. P. & Forester, R. W. (1971). Low-^{18}O igneous rocks from the intrusive complexes of Skye, Mull, and Ardnamurchan, western Scotland. *Journal of Petrology* **12**, 465–497.

Valley, J. W., Kitchen, N., Kohn, M. J., Niendorf, C. R. & Spicuzza, M. J. (1995). UWG-2, a garnet standard for oxygen isotope ratios: strategies for high precision and accuracy with laser heating. *Geochimica et Cosmochimica Acta* **59**, 5223–5231.

Vander Auwera, J., Bogaerts, M., Liégeois, J.-P., Demaiffe, D., Wilmart, E., Bolle, O. & Duchesne, J. C. (2003). Derivation of 1·0–0·9 Ga ferro-potassic A-type granitoids of southern Norway by extreme differentiation from basic magmas. *Precambrian Research* **124**, 107–148.

Vosteen, H. & Schellschmidt, R. (2003). Influence of temperature on thermal conductivity, thermal capacity and thermal diffusivity for different types of rocks. *Physics and Chemistry of the Earth* **28**, 499–509.

Wen, S. & Nekvasil, H. (1994). SOLVCALC: an interactive graphics program package for calculating the ternary feldspar solvus and for two-feldspar geothermometry. *Computers and Geosciences* **20**, 1025–1040.

Wenner, D. B. & Taylor, H. P. (1976). Oxygen and hydrogen isotope studies of a Precambrian granite–rhyolite terrane, St. Francois Mountains, southeastern Missouri. *Geological Society of America Bulletin* **87**, 1587–1598.

Whalen, J. B., Currie, K. L. & Chappell, B. W. (1987). A-type granites: geochemical characteristics, discrimination and petrogenesis. *Contributions to Mineralogy and Petrology* **95**, 407–419.

Williams, P. J., Barton, M. D., Johnson, D. A., Fontboté, L., de Haller, A., Mark, G., Oliver, N. H. S. & Marschik, R. (2005). Iron oxide copper–gold deposits: Geology, space–time distribution, and possible modes of origin. *Economic Geology, 100th Anniversary Volume* 371–405.

Yadav, O. P., Jain, R. B., Singh, R., Singh, G., Sharma, D. K. & Fahmi, S. (2000). Geology and geochemistry of uraniferous albitites of the middle Proterozoic Delhi Supergroup, Rajasthan, India. In: Gyani, K. C. & Katariya, P. (eds) *Tectonomagmatism, Geochemistry and Metamorphism of Precambrian Terrains*. Udaipur: Geology Department, Mohanlal Sukhadia University, pp. 303–320.

Zheng, Y. F. (1993). Calculation of oxygen isotope fractionation in anhydrous silicate minerals. *Geochimica et Cosmochimica Acta* **57**, 1079–1091.

APPENDIX

A granitoid body with an internal heat production greater than that of the surrounding region will heat up, or cool down, to a steady-state temperature distribution with a maximum temperature in the center of the body, which depends strongly on the size of the body. For simplicity, we make the following assumptions. The granitoid body is a sphere with radius a, a constant internal heat production A_0, a thermal conductivity K_0, and no contact resistance at its surface. It is surrounded by a country rock with zero heat production and a thermal conductivity K (here assumed to be identical to K_0). Although these assumptions seem highly idealized, such a treatment has the advantage of possessing a simple analytical solution (Carslaw & Jaeger, 1959), which gives good approximations to actual temperature distributions. For example, although radioactive heat production is not actually constant but declines with time, it can be treated as approximately constant over a period of 200–300 Myr. Also, little is known about the actual shapes of the granitoid bodies; however, the important parameter is size, not shape. The temperature T (given here as the temperature difference between the actual temperature and the ambient temperature of the region outside the granitoids) is given as a function of radius r, for the volume inside the body ($0 \le r < a$):

$$T = A_0[a^2 - r^2 + 2a^2(K_0/K)]/6K_0. \quad \text{(A1)}$$

For the region outside the granitoid body (i.e. $r > a$), the temperature is

$$T = A_0 a^3/3Kr \quad \text{(A2)}$$

(see Carslaw & Jaeger, 1959, Chapter IX, p. 232). We assume an internal heat production of $A_0 = 7{\cdot}5\ \mu\text{W m}^{-3}$, which is based on the following present-day concentrations of heat-producing elements: Th 34 ppm, U 8·5 ppm, K 3·1 wt %, assumed to be representative of the original granite. It should be noted that the uranium content assumed here is significantly higher than the measured U values, which are rather variable, leading to variable and high Th/U ratios, which are unlikely to be primary. We therefore assume that uranium has been removed by oxidation and dissolution, most probably by groundwater and weathering in recent times. Using the convenient formula by Beardsmore & Cull (2001) {heat production ($\mu\text{W m}^{-3}$) = $\rho(\text{g cm}^{-3})[0{\cdot}0967\text{U (ppm)} + 0{\cdot}0263\text{Th (ppm)} + 0{\cdot}035\,\text{K (wt \%)}]$}, and a density of $\rho = 2{\cdot}69\ (\text{g cm}^{-3})$, we obtain $4{\cdot}9\ \mu\text{W m}^{-3}$ for the present-day heat production of the original granite, slightly higher than the value of 4·1 given in Table 2 (owing to the use of the measured U value in that table). This value must be increased by about a factor of 1·5 to compensate for radioactive decay since 1·4–1·7 Ga. Thus we obtain a heat production value for the original granite of about $7{\cdot}5\ \mu\text{W m}^{-3}$, which is used for our calculation. The thermal conductivity K of granite at a temperature of 300°C is about $2{\cdot}3\ \text{W m}^{-1}\,\text{K}^{-1}$ (Vosteen & Schellschmidt, 2003).

Figure A1 shows the steady-state temperature calculated from equations (A1) and (A2) within and outside the spherical granitoid body for three radii (3, 6 and 10 km). Significant temperature increases over the ambient

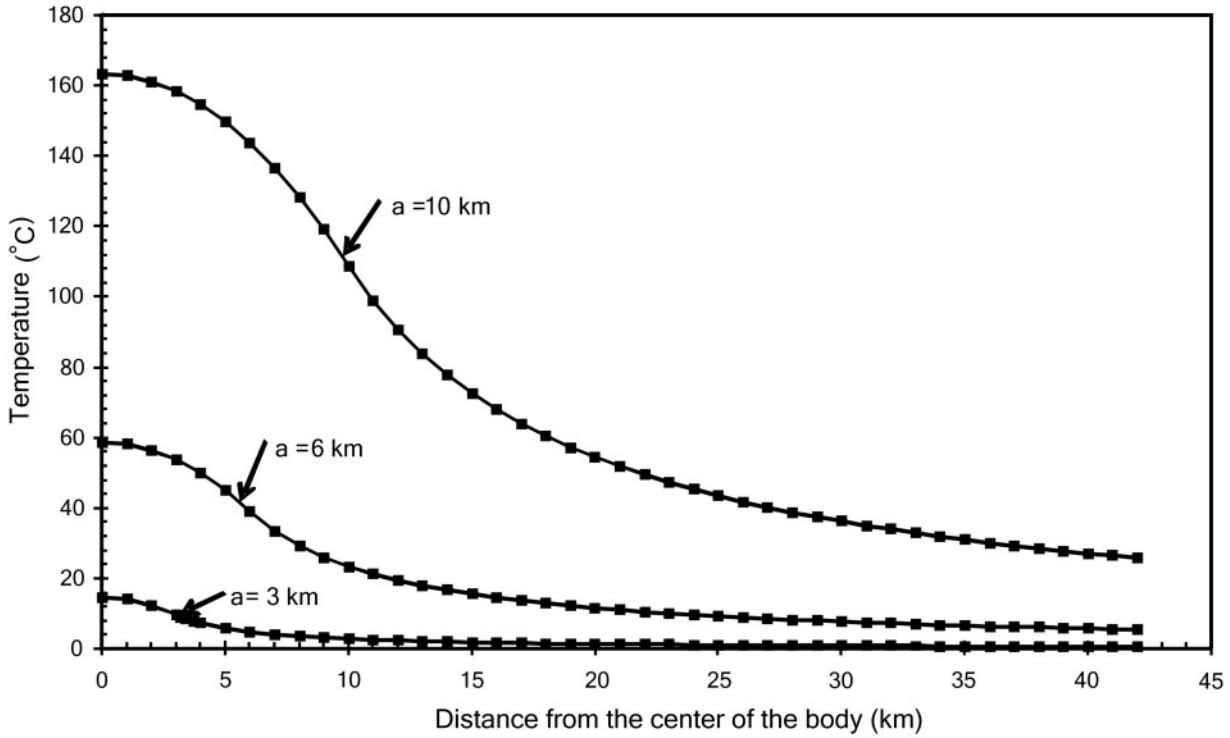

Fig. A1. Steady-state excess temperature (over the ambient temperature of the host-rock) for spherical granite bodies with radii of 3, 6, and 10 km and heat production of 7·5 $\mu W\ m^{-3}$ and a conductivity of 2·3 $W\ m^{-1} K^{-1}$.

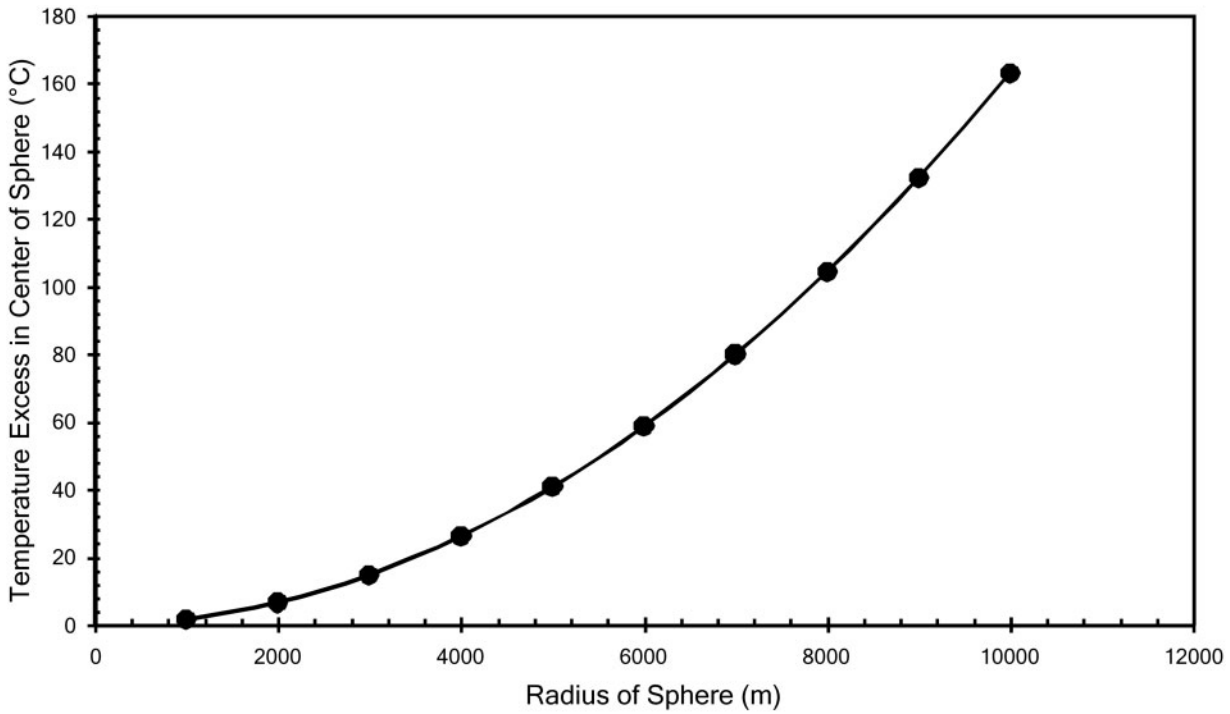

Fig. A2. Excess temperature in the center of spherical granitoid bodies as a function of radius of the body. Heat production and conductivity are the same as in Fig. A1.

temperature can be seen at distances up to at least four times the radius of the granitoid body. The curvature of the temperature distribution is inflected at the boundary. The temperature dependence on the radius of the body is plotted for the central temperature excess in Fig. A2. This illustrates the dramatic effect of the size of the body. The central temperature excess varies from nearly negligible for a radius of 1 km to very large (about 160°C) for a radius of 10 km. The effect would be even larger at higher ambient temperatures, because thermal conductivity decreases with increasing temperature (e.g. Vosteen & Schellschmidt, 2003). For example, at 500°C the thermal conductivity of the granitoid body is expected to drop to $2{\cdot}0\ W\ m^{-1}{}^{-}K^{-1}$, and the excess temperature in the center of the 10 km radius body would then be 190°C. Thus, the only way for a typical, highly Th–U-enriched (A-type) granite to escape such self-heating is by having small dimensions.